This is to certify that the

thesis entitled

DYNAMIC FLOW STUDY IN A FLOW OSCILLATING SYSTEM USING LASER DOPPLER VELOCIMETRY AND NUMERICAL SIMULATION

presented by

Xin Zhang

has been accepted towards fulfillment
of the requirements for

Master of Science degree in Mechanical Engineering

Major professor

Date August 25,2000

DYNAMIC FLOW STUDY IN A FLOW OSCILLATING SYSTEM USING LASER DOPPLER VELOCIMETRY AND NUMERICAL SIMULATION

By

Xin Zhang

A THESIS

Submitted to
Michigan State University
in partial fulfillment of the requirements
for the degree of

MASTER OF SCIENCE

Department of Mechanical Engineering

2000

ABSTRACT

DYNAMIC FLOW STUDY IN A FLOW OSCILLATING SYSTEM USING LASER DOPPLER VELOCIMETRY AND NUMERICAL SIMULATION

By

Xin Zhang

In this research, an air flow oscillator was used to simulate the air flow through an automotive induction system. The purpose of this research was to develop a better understanding of the flow characteristics of the oscillating flow in the test region by using both an experimental approach and a numerical simulation.

In the experiment part, Laser Doppler Velocimetry (LDV) was used to measure the velocity. Piezoresistive pressure sensor and amplifier were used to measure pressure distribution at different locations under different flow conditions. For the simulation part, Gridgen was applied to create the grid and STAR-CD was used to predict the flow characteristics under the same conditions. Both the experimental result and the STAR-CD modeling result lead to a better understanding of the flow condition in the flow oscillator system under different operating conditions. Also, comparison of the two different approaches was discussed and analyzed.

ACKNOWLEDGMENT

There are many people to whom I would like to express my appreciation. Their efforts and support help me complete this thesis. First, I would like to extend my sincere gratitude to Dr. Harold Schock, my academic advisor, for giving me opportunities and challenges of my graduate studies. I would not have been able to complete my studies without his guidance and financial support. Second, I would like to take the opportunity to thank many people who helped me grow academically and professionally; Dr. Brereton and Dr. Shih for being my committees and their great support, Dr. Keunchul Lee for his expertise with the LDV system, Tom Stuecken for his assistance with everything from repairing my test rig to helping me find a tool, Dr. Yuliang Lin for teaching me a large portion of grid generation, Shi Zheng for helping me use the STAR-CD software, and Bobbie Slider and Jan Chappell, for assistance on a daily basis. I would also like to thank my fellows at MSUERL, for their day to day guidance and their wonderful company; Mark Novak, Edward Timm, Steve George, Stephen Yen, Mahmood Rahi, Kyle Judd, Anthony Christie, Andrew Fedewa and Boon-Keat Chui. Finally, my brother Hui Zhang, for his patience and support throughout my master's program.

This thesis is dedicated to my parents

Yuanzong Zhang

&

Xiushu Zhao

For their love and support

TABLE OF CONTENTS

LIST OF FIGURES

LIST OF TABLES

LIST OF SYMBOLS AND ABBREVITIONS

The following is a list of definitions of the main symbols used in this thesis:

A	Area
BDC	Bottom Dead Center
CA	Crank angle
dp	Fringe spacing
e	Mechanical plus thermal energy per unit volume
i	Cycle number
k	Turbulent kinetic energy
l	Mixing length
Nc	Number of cycle
P	Pressure
q_i	Effective conduction in the i th direction
Re	Reynolds number
TDC	Top Dead Center
TI	Turbulent Intensity
U(t)	Instantaneous velocity
$\overline{U(t)}$	Mean velocity
$U_{EA}(\theta$	Ensemble averaged mean velocity
$u'_{ea}(\theta)$	Ensemble average fluctuation

θ	Crank angle
κ	Half angle between beams
λ	Wavelength of the laser light
ρ	Air density
τ_{ij}	Effective shear stress

CHAPTER 1. INTRODUCTION

1.1 Motivation

Competition in the automotive industry has increased the need to develop technology for superior engines. The automobile internal combustion engine has seen much advancement over the past twenty years. Much of this advancement has been to make engines more fuel efficient and cleaner burning to preserve the environment and bring rapid development to engine control and fuel injection systems. In order to have precise computer controlled fuel injection, there must be a means to measure the mass of air flowing into a vehicle's engine, such as the modern Mass Air Flow Sensor (MAFS). The Michigan State University Engine Research Laboratory has been previously involved in characterization the flows in a MAFS. A dynamic oscillating device was used to evaluate the performance of the MAFS under pulsating air flow conditions. The purpose of this study was to get a better understanding of the flow characteristics of the oscillating flow in the test region using both experiment measurement and numerical simulation.

MAFS's are now a standard part on nearly every production vehicle. They are located downstream of an automobile's air filter, and just upstream of the intake manifold and fuel injection system, and their job is to measure the airflow into the engine to control fuel delivery. There is some controversy, however, over how well certain MAFS's actually measure air flow into an engine. To fully understand the controversy, one must have some understanding of the typical air flow through the engines intake system, in particular how the flow passes the MAFS. First, nearly every engine is designed with a certain amount of

valve overlap, meaning that for a small crank angle duration, both the intake and exhaust valves are held open. While the reasoning for this will not be addressed, it is important to recognize that in many circumstances this will cause a small amount of air to flow backwards through the intake manifold before the fresh charge is drawn into the cylinder. For many engine speeds this same phenomenon (although to a much smaller extent) will be exhibited once the piston reaches bottom dead center (BDC), because the intake valve is still open slightly past the piston's BDC position. The final result is flow oscillation through the intake system, which may cause a discrepancy between the measured and actual mass of air flowing past the MAFS.

1.2 Problem Definition

To develop a better understanding the flow phenomena within the flow oscillator system, Laser Doppler Velocimetry (LDV) was conducted to measure the velocity. A piezoresistive pressure sensor and amplifier were also used to measure the pressure distribution at different locations for different flow conditions.

Computational Fluid Dynamics (CFD) approach, STAR-CD as the solver was used to predict the flow characteristics at the same conditions using Gridgen as the grid generation tool. The adaptation of standard CFD modeling codes enables predicting the major flows patterns. Very small velocity gradients can be visualized by adjusting the grid spacing to the geometrical location of interest.

The availability of a comparable amount of measured velocity and pressure data has always been a problem in the verification process of any modeling results. The possibility to validate and improve the basic assumptions and boundary conditions of the actual model is interdependent with the accuracy and availability of velocity and pressure

results measured in the same conditions. Since in the test region, only one component velocity is dominant, the comparison was made only for the single component modeled and measured results.

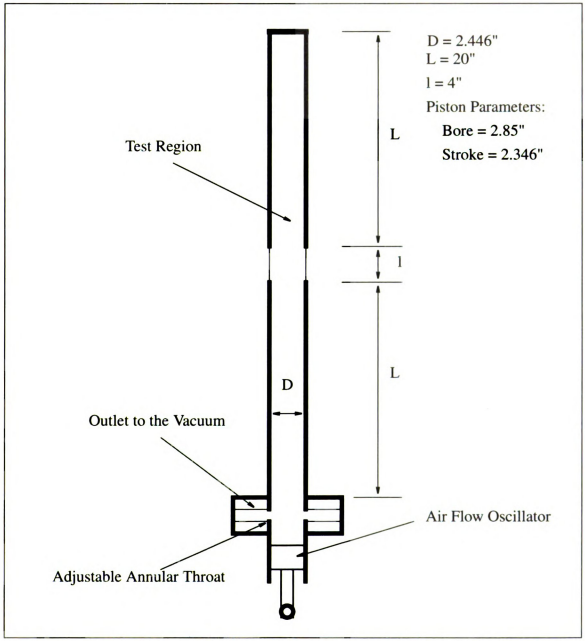

Figure 1: Schematic of the Flow Oscillator System

Figure 1 shows the schematic of the flow oscillator system in this study. The test region is consist of two 20 inches long clear acrylic round tubes with an optically clear quartz round tube in the middle of them. A single-cylinder engine was used to provide oscillating airflow. All the measurements and simulations were conducted at two engine speeds, 2000 rpm and 4000 rpm. The head assembly on the engine was removed and was replaced with an adjustable flow chamber. The flow chamber was configured with four outlets, which were connected to the vacuum accumulator tank by hoses. The flow rate can be increased or decreased by adjusting the flow chamber.

CHAPTER 2. EXPERIMENTAL TECHNIQUES AND FACILITIES

2.1 Test Rig

The measurements were conducted on a test bench that consisted of a test stand, single-cylinder flow oscillator, 10-hp DC electric motor, adjustable flow chamber and accumulator vacuum tank. The system is shown in Figure 2.

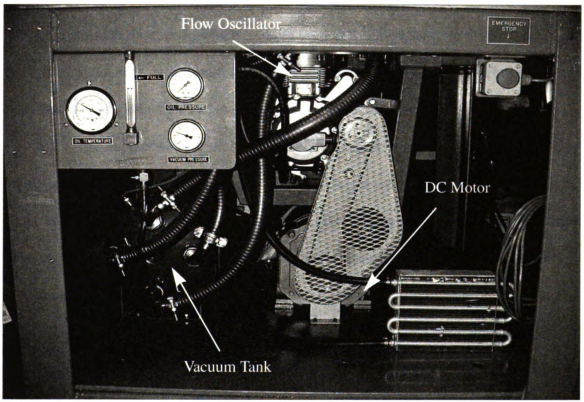

Figure 2: Flow Oscillator Test Rig

The single-cylinder flow oscillator was designed and built here at the MSU Engine Research Laboratory (ERL). As stated earlier, an internal combustion engine (IC) exhibits slight amounts of flow reversal in the intake manifold, and the flow reversal

effects are increased as the number of firing cylinders decreases. To simulate this phenomenon in a laboratory setting, a special test stand was built for laser diagnostics. The flow oscillator was designed to create small velocity oscillations in a flow with a given net velocity. To achieve this, a setup was built consisting of a large vacuum pump, and a small, single cylinder Suzuki engine (no head or valvetrain) and a DC motor. The vacuum pump creates a net velocity past the flow chamber (flow velocity can be controlled with the adjustable flow modulator above the 4-stroke engine to simulate engines of different size, number of cylinders, and operating speeds.), with the reciprocating piston imbedding a sinusoidal oscillation in the mean stream velocity. This oscillating air flow is drawn through a clear acrylic tube in which a quartz section. Located between the flow oscillator and the acrylic tube is a small section of aluminum honeycomb which serves two functions: to straighten flow and to prevent debris from falling onto the piston face.

The engine was driven by a 10-hp DC electric motor. Flows were examined based on the crank angle, which is detected by an angle encoder installer directly on the crankshaft. The encoder generates two series of 1024 square pulses per revolution. These two series of pulses are offset a half pulse length from each other. The data acquisition system can count 4 times the number of pulses from these two series of pulses. For this study, 4096 pulses per revolution (360 crank angle degrees) were used, which represents 0.088 degrees of angular resolution. The encoder was set to trigger when the piston in the engine was at Bottom Dead Center (BDC).

2.2 Laser Doppler Velocimetry System

2.2.1 Laser Doppler Velocimetry Technique Introduction

LDV has been used for non-intrusive flow studies for many years and is one of a very small group of technologies that can measure flows within closed systems. It requires no calibration under changing conditions and measures flows, without affecting the fluid flow. It uses only light and non-homogeneous scattering particle to obtain velocity measurements.

Laser Doppler theory states that the velocity of a particle can be measured by detecting the Doppler shift frequency of laser light scattered by the particle. The capability of the seed particle to follow flow characteristics was determined by determining the sedimentation velocity calculating the distance the particle has dropped due to gravitational forces in a flow of a known velocity over a given distance. If this vertical distance is less than 20% of the fixed distance through the given distance, the particle shows acceptable characteristics for following that flow velocity.

LDV technique relies on the light scattered by scattering centers in the fluid to measure flow velocity. In the following, the scattering centers will be referred to as particles, with the understanding that bubbles or anything else that has a relative refractive index (compared to the fluid) different from unity could be the source of scattered light. The particles, whose velocities are measured, must be small enough (generally in the micron range) to follow the flow and large enough to provide signal strength adequate for the signal processor to give velocity measurements. It should be noted that the signal exists only when a detectable particle is in the measuring volume and, hence, is discontinuous.

The dual-beam approach is the most common optical arrangement used for LDV system for flow measurement applications. The scattered light is collected by a photomultiplier. The function of the photomultiplier is to convert bursts of light scattered in the fringe pattern into an analog signal for interpretation by the data acquisition equipment (IFA-750). The data acquisition equipment then combines the frequency of the analog signals with a set of encoder values relating to the position of the impeller and turbine. This related data set is stored in a PC connected to the data acquisition hardware. The system which we were using is a back-scattering system, where the burst of light scattered from the measurement volume are collected at a physical location in front of the focal point. In back-scatter mode, the intensity of scattered light is weaker than scattered light intensities using the forward-scattering method. Back-scatter data collection was used in this experiment due to optical access constraints.

The point of measurement is a volume determined by the half angle of the beams (κ) intersecting at the focal point and the wavelength of light used (λ). This volume is in the shape of an ellipsoid with the length governed by Equation 1. The height of the ellipsoid is determined by Equation 2.

$$l_m = \frac{4f\lambda}{\pi D_{e^{-2}} \sin\kappa} \tag{1}$$

$$d_m = \frac{4f\lambda}{\pi D_{e^{-2}} \cos\kappa} \tag{2}$$

The measurement volume is thus defined by Equation 3.

$$V = \left(\frac{(4f\lambda)^3}{D_{e^{-2}}^3 \pi^2} \cdot \frac{1}{6((\cos\kappa)^2 \cdot \sin\kappa)} \right) \quad (3)$$

Where f is the focal length, λ represents the wavelength of the light used and D_e^{-2} represents the diameter of the unfocused Gaussian laser beam measured at $1/e^{-2}$ of the center line intensity. The frequency of the signal converted by the photodetector increases in proportion to the half angle value. Therefore, the half angle can limit the range of measurable velocities. Velocity measurements have been made from $1\mu m$/sec to 1000 m/s. This wide range of measurements is made possible, in part, by changing the half angle to allow for measurement of the velocity range. The half angle generates a fringe pattern when two beams of polarized laser light interfere with each other at the focal point.

As the beams of the unshifted and that of shifted beam cross, a fringe pattern moving in a know direction, is formed. Shifting the frequency of a laser beam refers to changing the frequency of the laser light by a known quantity either up or down. Frequency shifting is commonly used in LDV measurements. The purpose for this is to measure flow reversal, to measure small component velocities in the presence of large component velocities and to increase the range of velocities that can be measured by the signal processor. The frequency of the signal collected by the signal processor is fixed at 40MHz by a Bragg cell. This frequency is then down mixed to a value greater than twice the Doppler frequency for the corresponding negative velocity. The direction of the fringe motion is normally oriented in a direction opposing the mean positive flow. Thus any velocity measured that has a frequency less than the shift value is negative and those with greater frequencies are positive. The formula use to resolve positive and negative velocity measurements is represented by Equation 4.The velocity value used in Equation 4 is

determined by the result of Equation 5. The Doppler frequency is simply the frequency at which the signal processor receives light burst signals from the incidence of seed particles passing through the focal point.

$$\text{Frequency} = \text{Shift Frequecy} \pm \frac{|\text{Velocity}|}{\text{Fringe Spacing}} \tag{4}$$

$$\text{Velocity} = \text{Doppler Frequency} \cdot \text{Fringe Space} \tag{5}$$

The data acquisition equipment has been pre-programed with the characteristics of the laser beam and its shift parameters. The data acquisition equipment calculates the fringe spacing using the wavelength of the laser light and the half angle between the beams as seen Equation 6.

$$d_f = \frac{\lambda}{2\sin\kappa} \tag{6}$$

The velocity of the particle passing through the fringe pattern is then calculated by multiplying the fringe spacing by the frequency of the Doppler shifted light scattered by the particle. The frequency of Doppler shifted light is equal to the number of fringe patterns scattered in a fixed amount of time over a known distance and is measured in Hertz (Hz). This information can then be used to infer direction and velocity directly by noting the orientation of the shifted beam to the unshifted beam and their orientation in Cartesian space. These calculations are carried out in the IFA 750 signal processor which collects data from all the sensing equipment used. The information regarding the adjusted frequency, representing the velocity of the particles through the measurement volume, is then stored in a PC running TSI FIND™ data acquisition software. This software is used to control and program the data acquisition equipment.

The laser used was a multi-frequency Argon-ion laser capable of producing three wave lengths of light. The wave lengths of light are green at 514.5 nm, blue at 488 nm and violet at 476.5 nm. This experiment used the green wavelength. These wavelengths are separated by a device called the Colorburst, manufactured by TSI. It is composed of a set of optics used as beam splitters for certain wavelength of light. Once separated, each distinct wavelength of laser light can be routed via fiber optics to the LDV probe face where their orientation, on the face of the probe, determine which velocity components they will measure.

The proper selection of particles can have a strong influence on the quality of the data in the LDV system. For most experimentalists, the first reaction is to rely on particles naturally present in the flow. This may be adequate in some of the applications, e.g., forward scatter in water. In almost all other cases, it is generally desirable to seed the flow suitably to get adequate data rates. Several techniques give data in forward scatter, Fluorescent particle work in backscatter. There is no universal solution but acceptable particles and technique normally are available for a given application.

2.2.2 Ensemble Averaged Mean Velocity

An important characteristic of periodic flow is ensemble-averaged mean velocity. The statistical description of periodic flow is conventionally used for engine studies. Although the flow visualization technique can determine bulk features, the differences between features are often subtle and can not be described in a quantitative way. Therefore quantitative analysis is important to understand the flow characteristics in a highly fluctuating turbulent flow like the one in the oscillating flow system. One of the important characteristics of turbulent flow is that of its irregularity or randomness.

Statistical methods are used to define such flow field. The quantities that characterize turbulence are usually the mean velocity and the fluctuation velocity about the mean, and length and time scale. The local instaneous velocity can be defined by Equation 7.

$$U(t) = \bar{U} + u'(t) \tag{7}$$

Here the mean velocity is the time average of $U(t)$. It is shown in Equation 8.

$$\bar{U} = \lim_{\tau \to \infty} \frac{1}{\tau} \int_{t_0}^{(t_0 + \tau)} U(t) \tag{8}$$

The turbulent portion of the velocity is $u'(t)$. For a steady flow, the mean stands for the simple time averaged value. In this steady, the mean value can vary significantly from one engine cycle to the next. Instantaneous velocity can be written as a function of cam angle θ and cycle number instead of a function of time, which is shown in Equation 9.

$$U(\theta, i) = \bar{U}(\theta, i) + u'(\theta, i) \tag{9}$$

The ensemble averaged velocity $U_{ea}(\theta)$ over Nc cycles can be defined as:

$$\bar{U}_{ea}(\theta) = \frac{1}{Nc} \sum_{1}^{Nc} U(\theta, i) \tag{10}$$

Where the Nc is the number of cycles for which data is available. The ensemble average velocity is only a function of cam angle since the cyclic variation has been averaged out. The difference between the mean velocity in a particular cycle and the ensemble averaged mean velocity over many cycles is defined as the cycle by cycle variation in mean velocity:

$$\hat{U}(\theta, i) = \bar{U}(\theta, i) - \bar{U}_{ea}(\theta, i) \tag{11}$$

Thus the instaneous velocity can be split into three components:

$$U(\theta, i) = \overline{U}_{ea}(\theta, i) + \hat{U}(\theta, i) + u'(\theta, i) \tag{12}$$

This is the most desirable equation to be used for the measuring velocity in the study. The ensemble averaged fluctuation $u'_{ea}(\theta)$ is given by:

$$u'_{ea}(\theta) = \frac{1}{Nc}\sum_{1}^{Nc} u'(\theta, i) \tag{13}$$

It includes all fluctuations about the ensemble averaged mean velocity. Based upon Equation (12) and (13), ensemble averaged mean velocity and mean fluctuation were calculated.

2.2.3 Laser Doppler Velocimetry System Overview

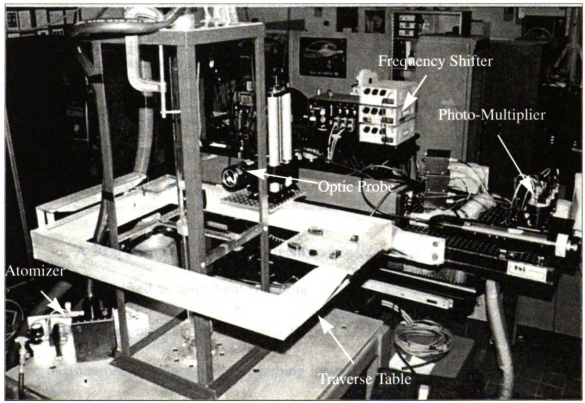

Figure 3: LDV System Setup

A single-component Laser Doppler Velocimetry (LDV) system was utilized in determining the velocity profiles in this experiment. Elements making up the LDV include an Argon-ion laser, beam collimator, Colorburst Multicolor Beam Separator (TSI), LV Frequency Shifter, 4-beam fiber optic probe with transmitting and receiving optics, photomultiplier, digital burst correlator (TSI, IFA 750), rotating machine resolver (RMR), traverse mechanism (for moving and focusing the laser beams), and computer for data collection and storage are also required for this experiment. The system is shown in Figure 3

The single-component LDV system is using the green beams (shifted beam and unshifted beam). The laser optical parameter is shown is Table 1.

Table 1: Laser Optical Parameters (For green laser beams)

Laser Optical Parameters	Green Laser Beams
Laser Wave Length (nm)	514.5
Beam Spacing (mm)	50
Focal Length (mm)	261
Half Angle κ (degree)	5.52
Fringe Spacing (μm)	2.674

A 20% mixture of propylene glycol and water mixture was atomized by a Six-Jet Atomizer and used as laser light scattering particles. The diameters of the particles generated by the atomizer are in the range of 0.6 to 1.5 μm. These particles were supplied to the measurement region without disturbing the airflow generated by the engine. The Six-Jet Atomizer and the hose for inducting the seeding flow were shown in Figure 4.

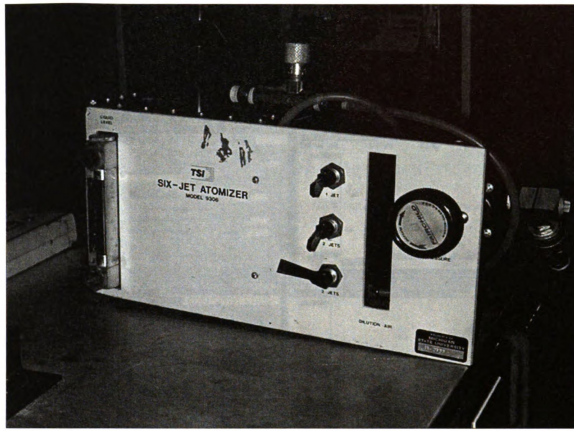

Figure 4: Six-Jet Atomizer

2.2.4 Data Acquisition And Data Analysis System

FIND™ was used as the signal processing software for the LDV system. FIND™ stands for Flow Information Display. It is a Windows-based data acquisition and analysis software that is part of TSI's integrated Laser Doppler Velocimetry (LDV) and Adaptive Phase/Doppler Velocimetry (APV) systems. Comparing the old DOS version system, it has a lot of advantages. FIND™ is easier to set up the experiment parameters and the true multiple Real-time View Display gives more control to the experiment. The post-processing work is made much easier by the Statistical Analysis tool. Statistical results can viewed as tabular data, spreadsheet row column, or graphically using the built-

in graphics display. FIND™ for Windows Version 1.4 Graphical User Interface is shown in Figure 5 below.

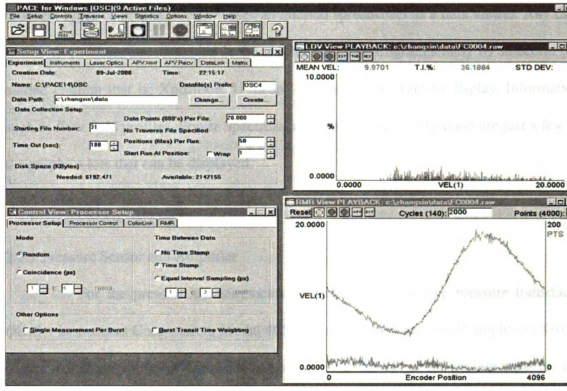

Figure 5: FIND™ for Windows Version 1.4 Graphical User Interface

FIND™ performs all hardware interfacing functions and runs the software diagnostics to make sure the hardware is operation correctly. Since it operates in real time, you can get instantaneous feedback on various parameter settings and make adjustments before station the actual experiment.

FIND™ provides complete flow statistics for every measurement point. It calculates and displays all basic flow statistics, including mean velocity, standard deviation, turbulence intensity, shear stress, and correlation coefficients for up to three velocity components. Since raw data is accessible to other statistical programs, the user

can use it for any other type of calculations. Data can also be collected as a function of time to provide time series information.

FIND™ has a built-in graphics display capability that can display many different types of graphs. FIND™ uses an internal spreadsheet as a data viewer. Any data in this spreadsheet can displayed in the graphics display program simply by selection (by named column that is: Xposition, U-mean, etc.) what you want to display. Information such as flow field profiles, Power Spectrum, and particle-size distribution are just a few of the graphics lots that can be displayed.

2.3 Pressure Measurement System

2.3.1 Pressure Sensor and Amplifier

For the pressure measurements, a Kistler piezoresistive pressure transducer (Kistler Instrument Cooperation, Model 4053A2) and Kistler dual mode amplifier (Kistler Instrument Cooperation, Model 4618A0) were used. Details of the system used for the pressure measurements are shown in Table 2.

Table 2: Pressure Measurement System

Component/Specification	Description	
	SI unit	English unit
Pressure Transducer	Kistler Instrument Cooperation, Model 4053A2	
Amplifier	Kistler Instrument Cooperation, Model 4618A0	
Measurement Range	0 - 200 kpa_{rel}	0 - 2 bar_{rel}
Sensitivity	1.25 mV/kpa	250 mV/bar
Calibration Current	2 - 5 mA	

Table 2: Pressure Measurement System

Component/Specification	Description	
	SI unit	English unit
Compensated Temperature Range	-20 - 70 C	
Amplifier Supply	+18 - 30V DC	

2.3.2 Data Acquisition System

The Real Time Combustion Analysis Module (RTCAM) system collects all the pressure vs. crank angle data from the engine. Using the piezoresistive pressure transducer, along with the BEI optical shaft encoder (OSE), the system can display pressure as a function of crank angle in real time, allowing effects of injection and ignition timing changes to be easily observed. The pressure vs. crank angle data (for a specified number of engine cycles) can also be permanently recorded in ASCII file format.

The Real Time Combustion Analysis Module acquires cylinder pressure and other analog and digital data from single or multiple cylinder engines. Calculating the parameters from the cylinder pressure data on-line while the engine is running is a key future of real time analysis. This will reduce the volume of data required to be stored by extracting information from the data and on.y storing the results. For this measurements, twenty cycles of pressure data were collected when a trigger event occurred. The trigger event was configured by the optical shaft encoder signal. Then the averaged value for each crank angle was calculated by the system. The schematic of the pressure measurement system can be seen in Figure 6.

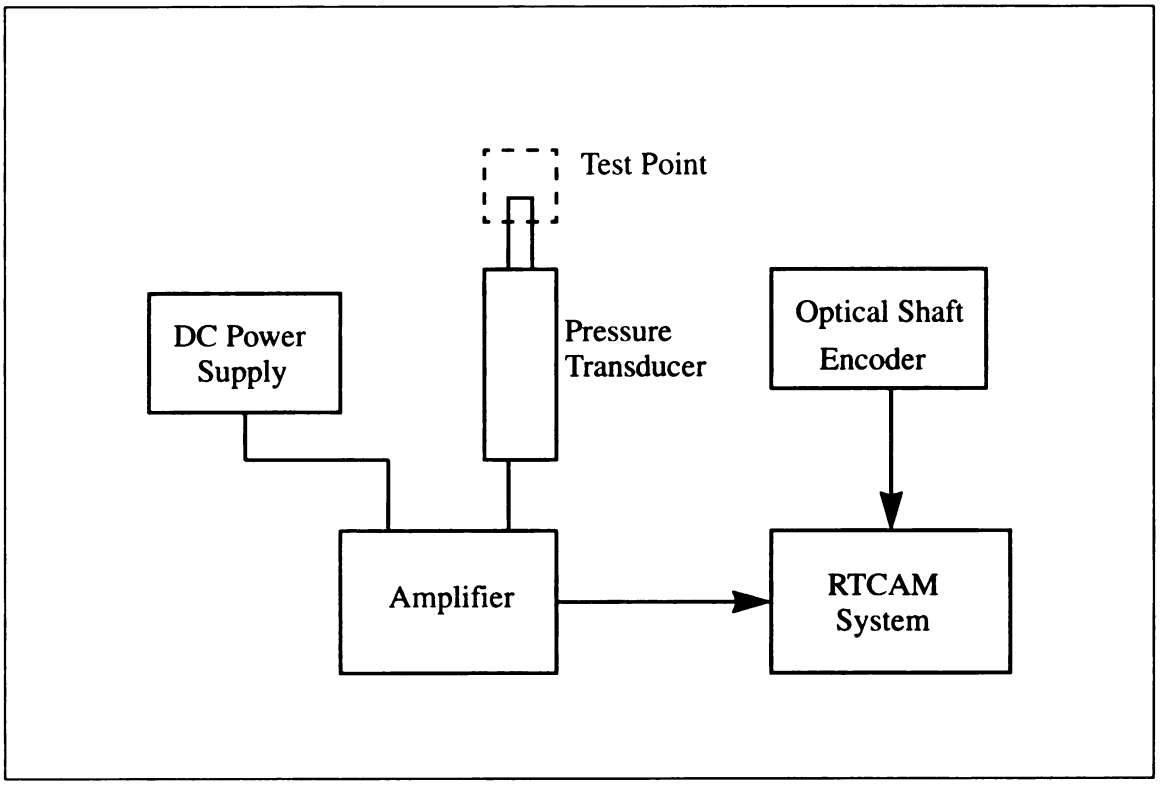

Figure 6: Pressure Measurement System Setup

CHAPTER 3. EXPERIMENTAL PROCEDURE

3.1 Coordinate Systems

The LDV traverse table system is designed for translation in three dimensions. It is equipped with stepper motors for automated translation with a maximum resolution of 1 μm. The local coordinate system is set by the LDV traverse table and requires a reference point for all of its translational movement to be relative to. Setting the local coordinate system is done by positioning the LDV laser focal point on the test stand or converter itself and referencing the local coordinate system from that location. Both the LDV measurement and the pressure measurement are only along the Z-direction of the local coordinate system. It is also the main air flow direction in the measurements.

The measurements were conducted on three different locations in the test region. They were measured from the piston top in the flow oscillator system when the piston was at bottom dead center (BDC). The distances were 12 inches, 25 inches and 43 inches respectively. The origin was located in the center of the piston top surface. Since the direction of most of the velocity measurements was toward the piston top because of the offset flow created by the vacuum pump, it is convenient to define the downward direction as the positive direction of the velocity measurements.

The local coordinate system and the three locations can be seen in Figure 7.

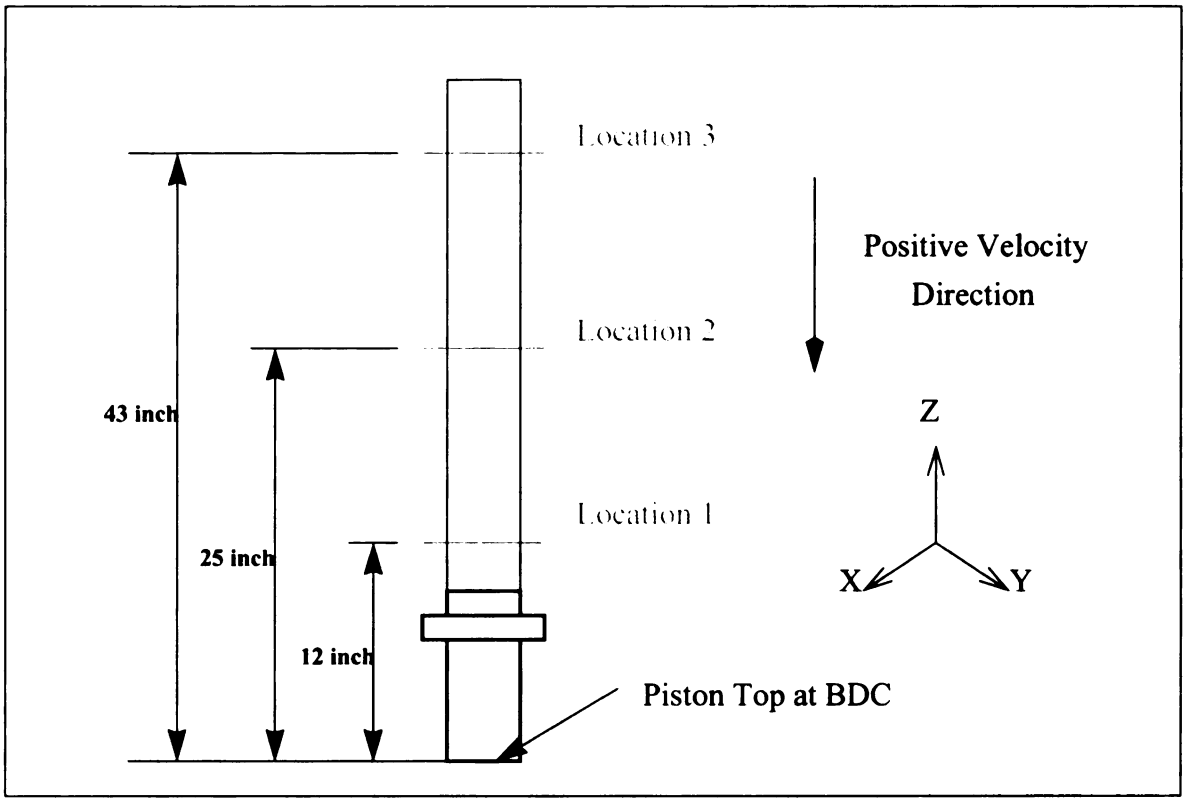

Figure 7: The Local Coordinate System and the Three Measured Locations

3.2 LDV Measurement

3.2.1 Experiment Sequence

Prior to collection the LDV data, the system was turned on by following a specified sequence of steps. First, the vacuum used to provide the offset airflow was turned on and the atomized seeding particles were introduced into the airflow. The DC motor was then activated and the engine was brought up to two different speeds, 2000 rpm and 4000 rpm respectively. The LDV system was then utilized to measure the ensemble averaged velocity at three different locations. Once one flow rate was finished, the air flow was adjusted to another flow rate and the same procedures were repeated.

3.2.2 LDV Data Collection

Three different flow rates and three different locations were measured under two engine speeds, 2000 rpm and 4000 rpm respectively. The three locations are shown in Figure 7. For location 1, only one flow rate (Flow Rate 2) was measured because it was very near the oscillator and the seeding flow was really difficult to get in there. The signal and data rate was very bad down there. For location 2 and 3, data were collected at five points across the test region (x=-20mm, -10mm, 0mm, 10mm, 20mm). The three different flow rates are shown in Table 3. All data were collected in 360 crank angle degrees. The encoder was set to trigger when the piston in the engine was at Bottom Dead Center (BDC).

Table 3: Three Different Flow Rates

	Velocity(m/s)	Area(m^2)	Flow Rate(m^3/s)	Flow Rate(g/s)
Flow Rate #1	5.3536	0.00219	0.0117	14.1
Flow Rate #2	10.1544	0.00219	0.0223	26.7
Flow Rate #3	31.6382	0.00219	0.0694	83.2

3.3 Pressure Measurement

The pressure measurement was conducting under the same three flow rates and two engine speeds as the LDV measurement.

The test system was initiated by a specific sequence of steps. First, the vacuum pump was turned on to create the offset flow. Then the DC motor was activated and the engine brought up to two different speeds, 2000 rpm and 4000 rpm respectively. The Real Time Combustion Analysis Module (RTCAM) system was used as the data acquisition

system and collected the pressure data as the function of the crank angle. The shaft encoder was set to trigger when the piston in the oscillator was at Bottom Dead Center (BDC). Once one flow rate was finished, the air flow was adjusted to another flow rate and the same procedures were repeated.

CHAPTER 4. EXPERIMENTAL RESULTS AND DISCUSSION

4.1 LDV Velocity Measurements

4.1.1 Velocity Measurements at 2000 rpm

Figure 8 shows flow velocities vs. crank angle at 2000 rpm for location 1 and flow rate 2. Because location 1 is the nearest measured point to the piston top in the test region, the seeding flow for the LDV measurement was difficult to be provided to that location. For higher engine speed, it was even more difficult. The results of these measurements suggested that the velocity profiles were almost similar across the test region. Image in this chapter of thesis are presented in color.

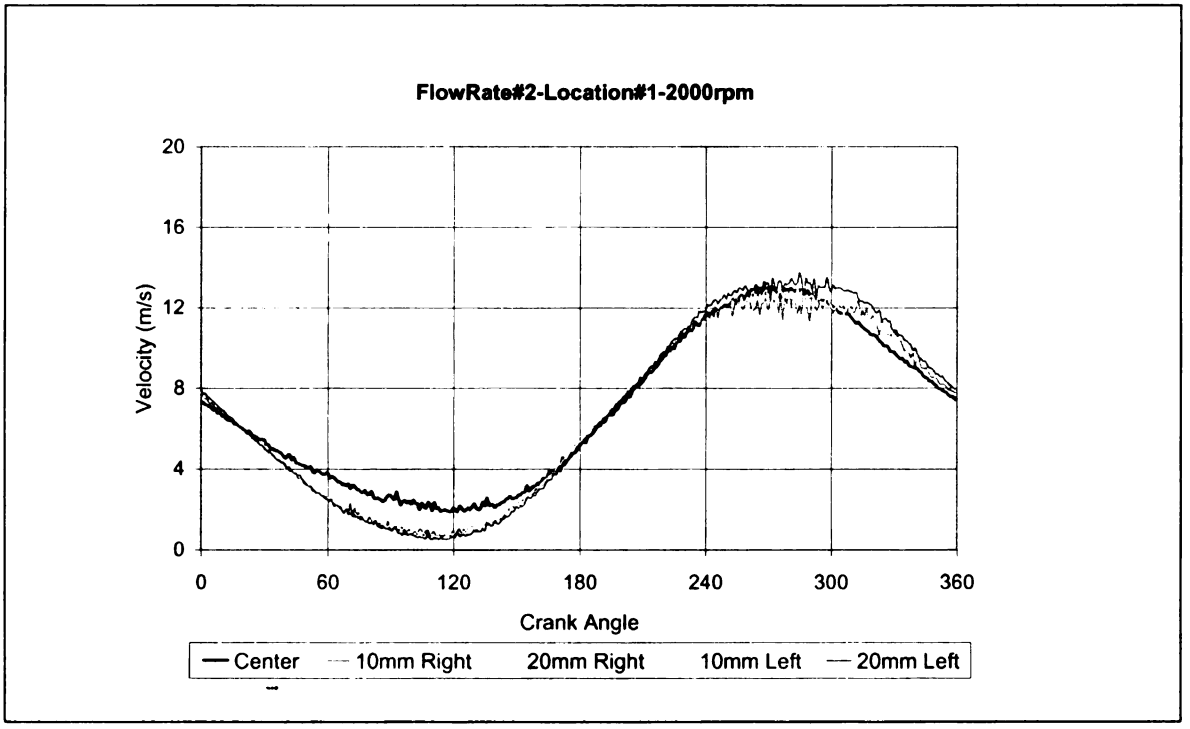

Figure 8: Velocity Profile at Location 1 (2000rpm, Flow Rate 2)

Figure 9, 10, 11 shows flow velocities vs. crank angle at 2000 rpm for location 2 and flow rate 1, 2 and 3, respectively. The velocity profiles are similar for three different flow rates. They all start at low velocity from crank angle at 0 degree, which piston moves from the BDC, and the highest velocities are appearing at about 270 degree. And all velocity curves are almost constants between 60 and 150 degrees. They are supposed to be the bottom of the sine wave. The reason is the offset flow created by the vacuum. When the piston moves up from the BDC, the flow is dragged back by the offset flow. As we can observe from the three plots, the velocity magnitudes increase as we increase the offset flow rate.

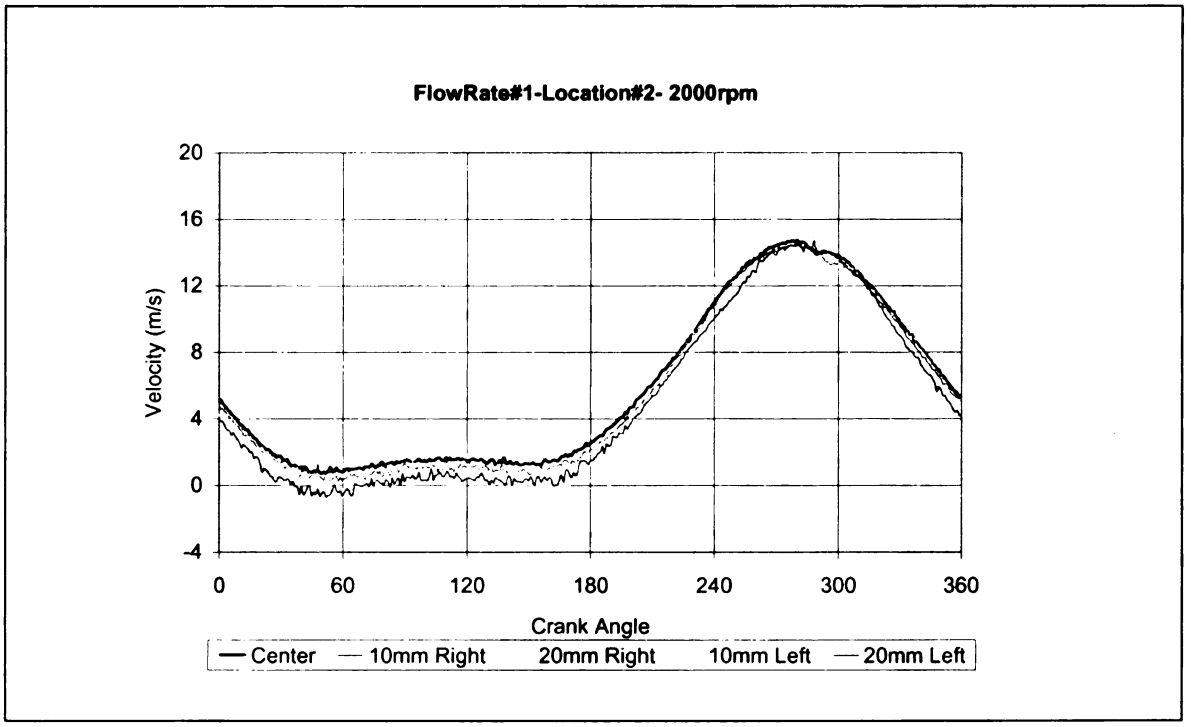

Figure 9: Velocity Profile at Location 2 (2000rpm, Flow Rate 1)

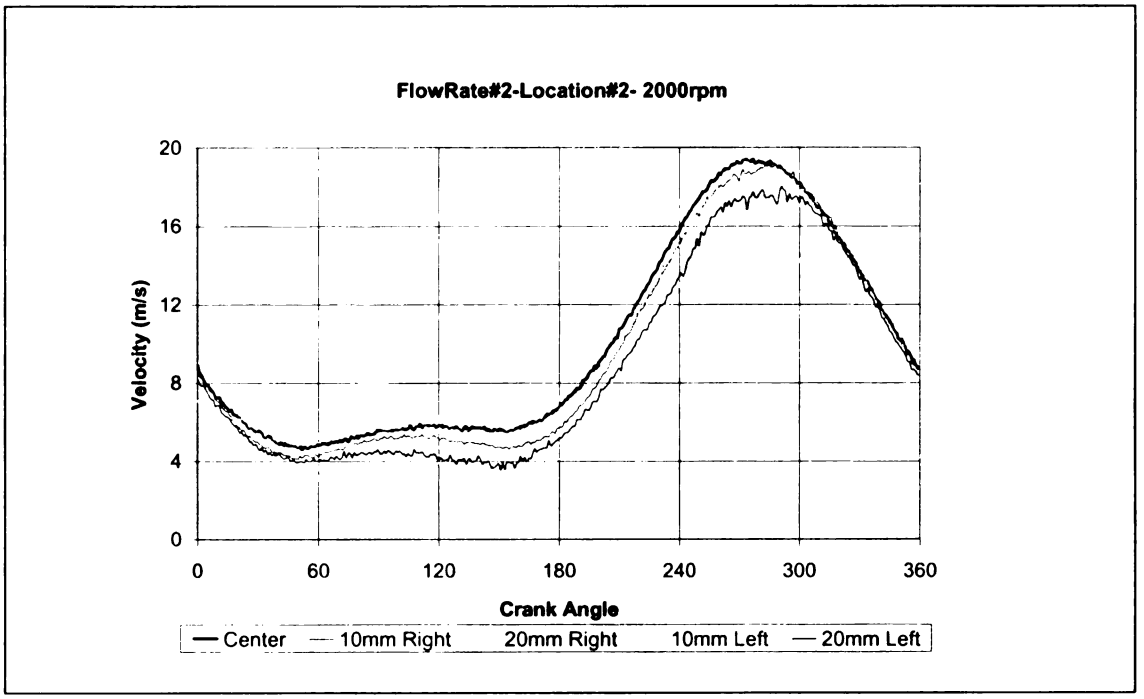

Figure 10: Velocity Profile at Location 2 (2000rpm, Flow Rate 2)

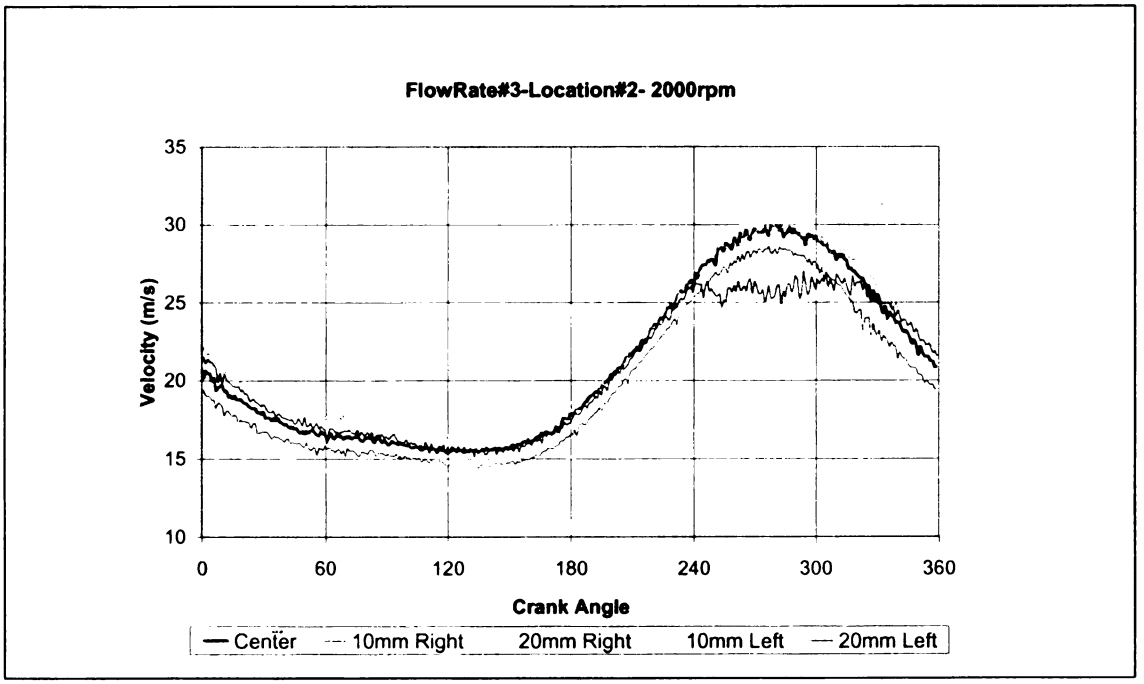

Figure 11: Velocity Profile at Location 2 (2000rpm, Flow Rate 3)

Figure 12, 13, 14 shows flow velocities vs. crank angle at 2000 rpm for location 3 and flow rate 1, 2 and 3, respectively. Comparing to the results at location 2, the velocity profiles show the same type of the curve and the characteristics for the highest and lowest velocities are also similar.

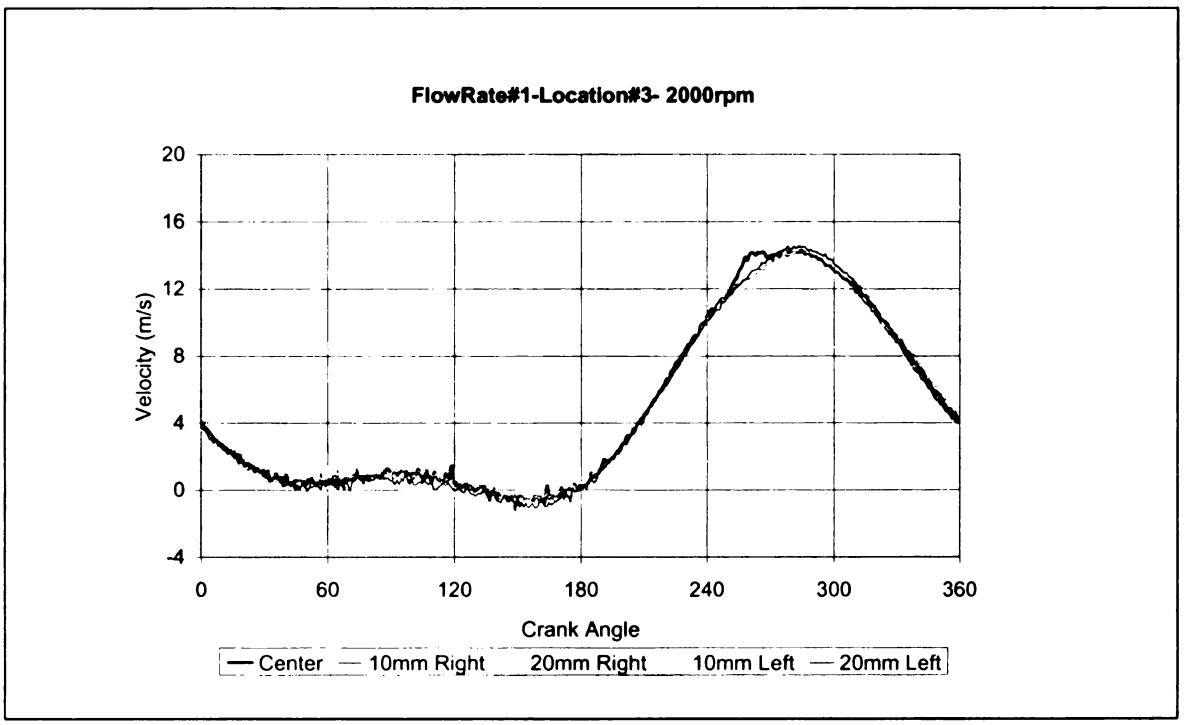

Figure 12: Velocity Profile at Location 3 (2000rpm, Flow Rate 1)

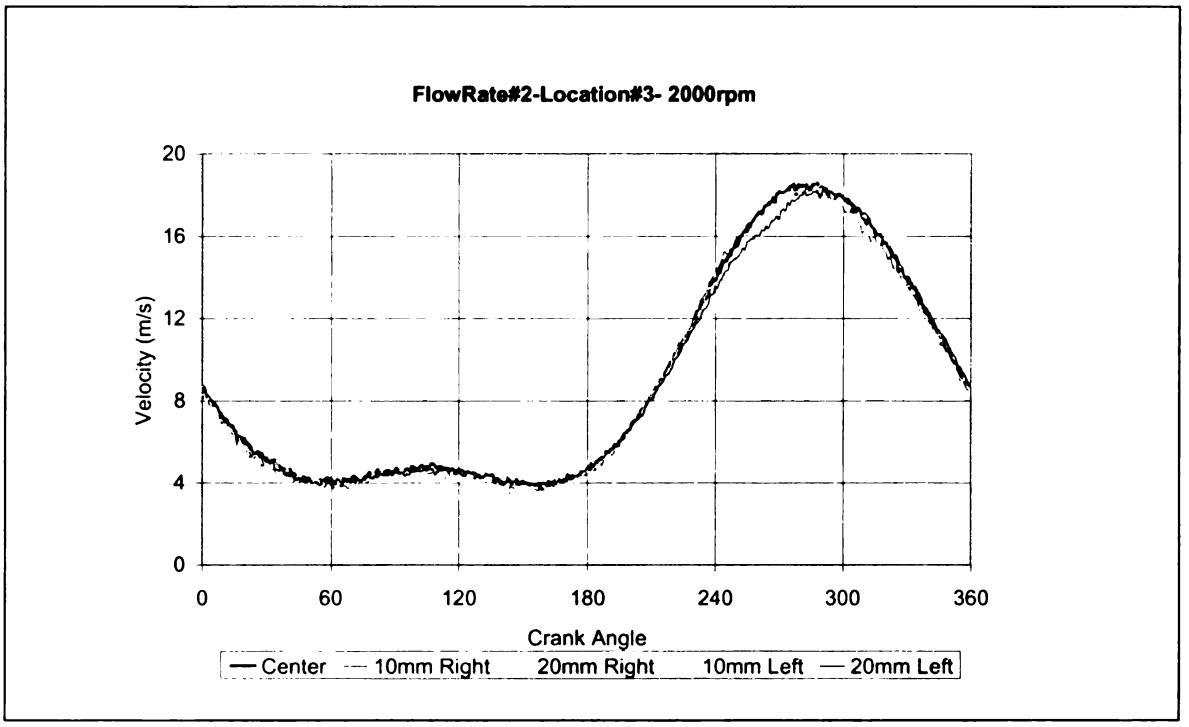

Figure 13: Velocity Profile at Location 3 (2000rpm, Flow Rate 2)

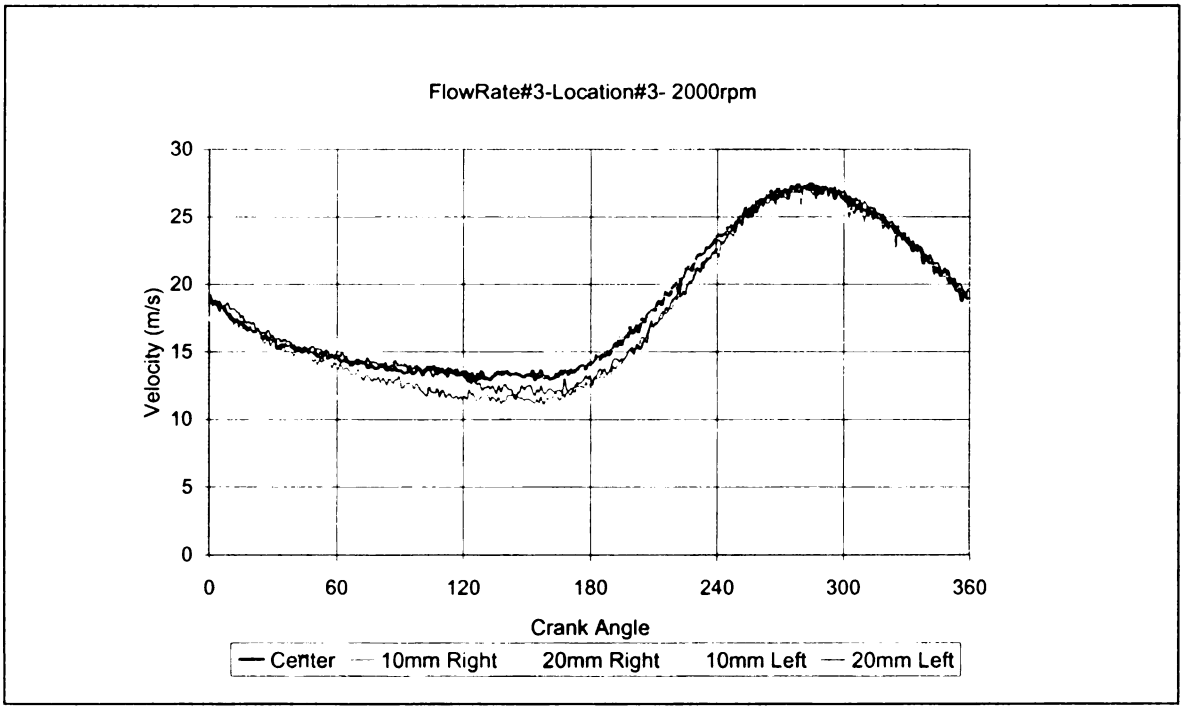

Figure 14: Velocity Profile at Location 3 (2000rpm, Flow Rate 3)

4.1.2 Velocity Measurements at 4000 rpm

Figure 15, 16, 17 shows flow velocities vs. crank angle at 4000 rpm for location 2 and flow rate 1, 2 and 3, respectively. Comparing to the velocity profiles at the same location at 2000 rpm, the curves look more like the sine wave. The reason for this is the increasing frequency piston movements overcome the offset flow created by the vacuum.

For flow rate 2 and 3, we can see the data collected by the LDV system have some fluctuations between crank angle 150 and 200 degree. This shows the flow characteristics at the time of changing the flow direction when piston move across the TDC.

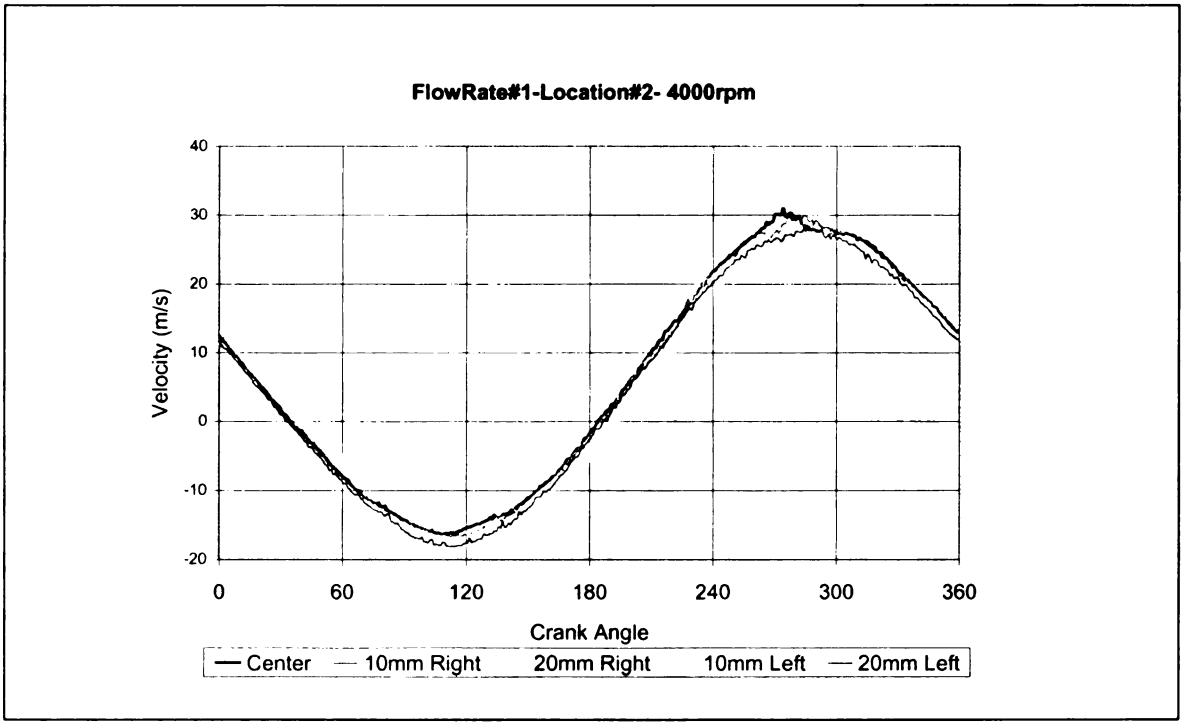

Figure 15: Velocity Profile at Location 2 (4000rpm, Flow Rate 1)

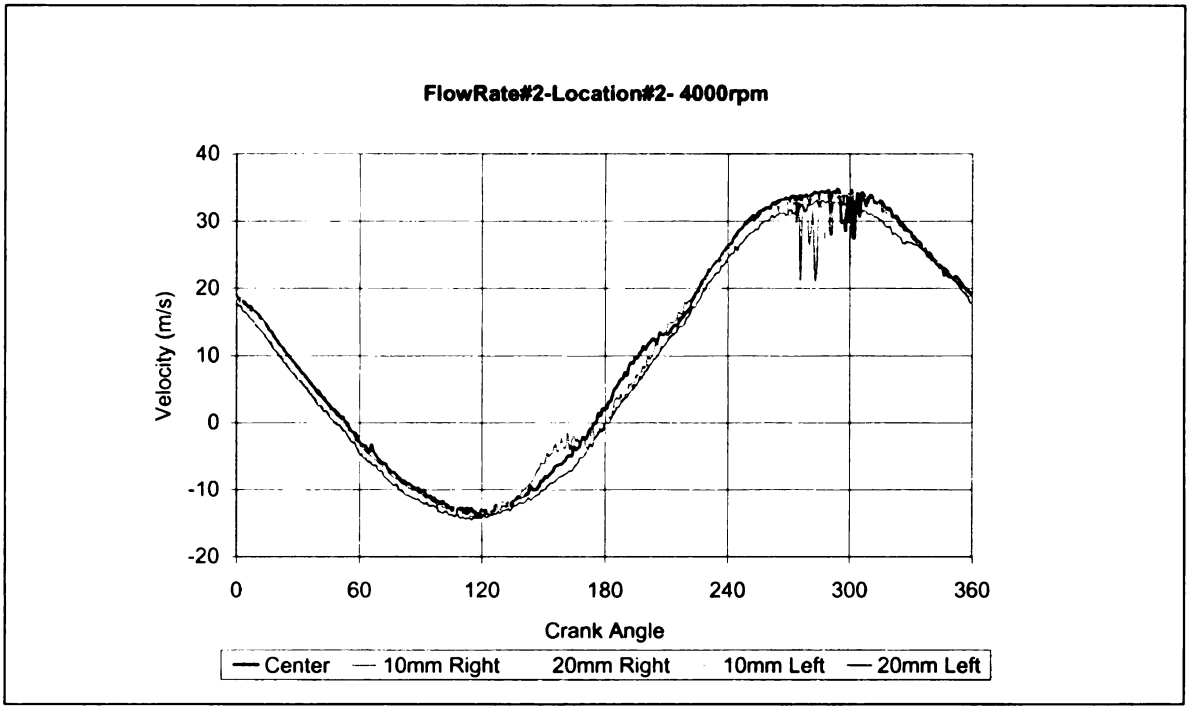

Figure 16: Velocity Profile at Location 2 (4000rpm, Flow Rate 2)

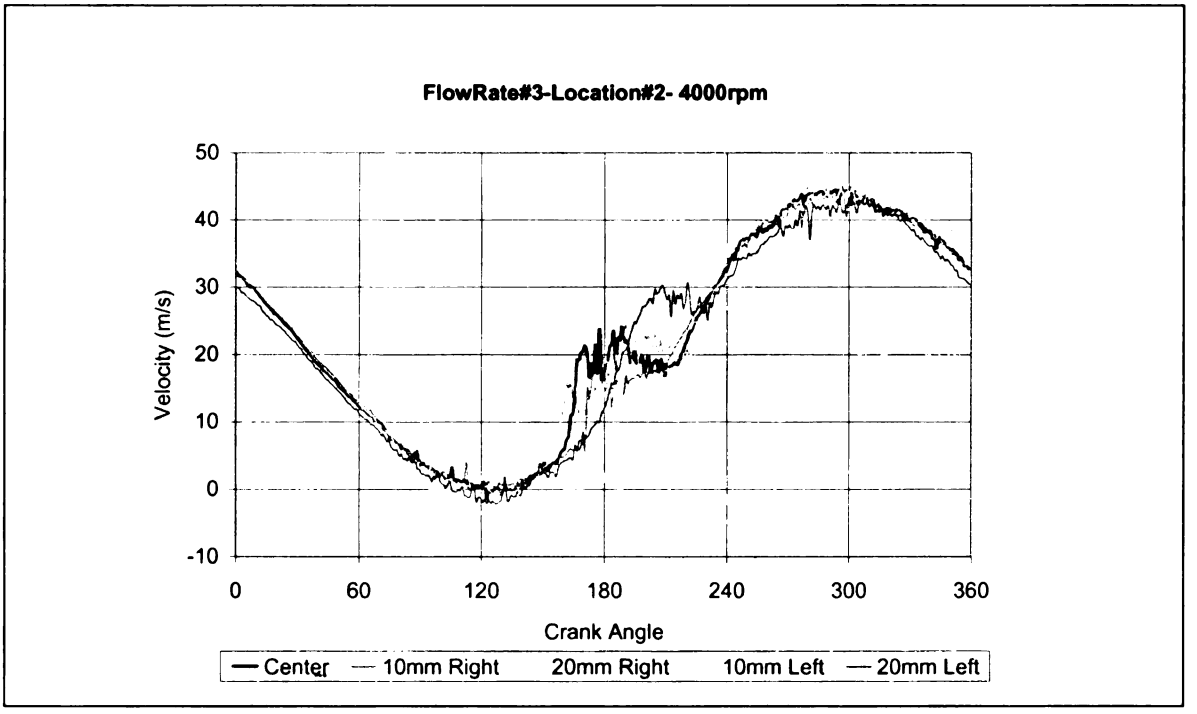

Figure 17: Velocity Profile at Location 2 (4000rpm, Flow Rate 3)

Figure 18, 19, 20 shows flow velocities vs. crank angle at 4000 rpm for location 3 and flow rate 1, 2 and 3, respectively. Comparing to the velocity profiles at the same location at 2000 rpm, the curves look more like the sine wave. The reason for this is the increasing frequency piston movements overcome the offset flow created by the vacuum. When comparing the velocity profiles at location 2 at the same engine speed, the velocity magnitude are almost the same.

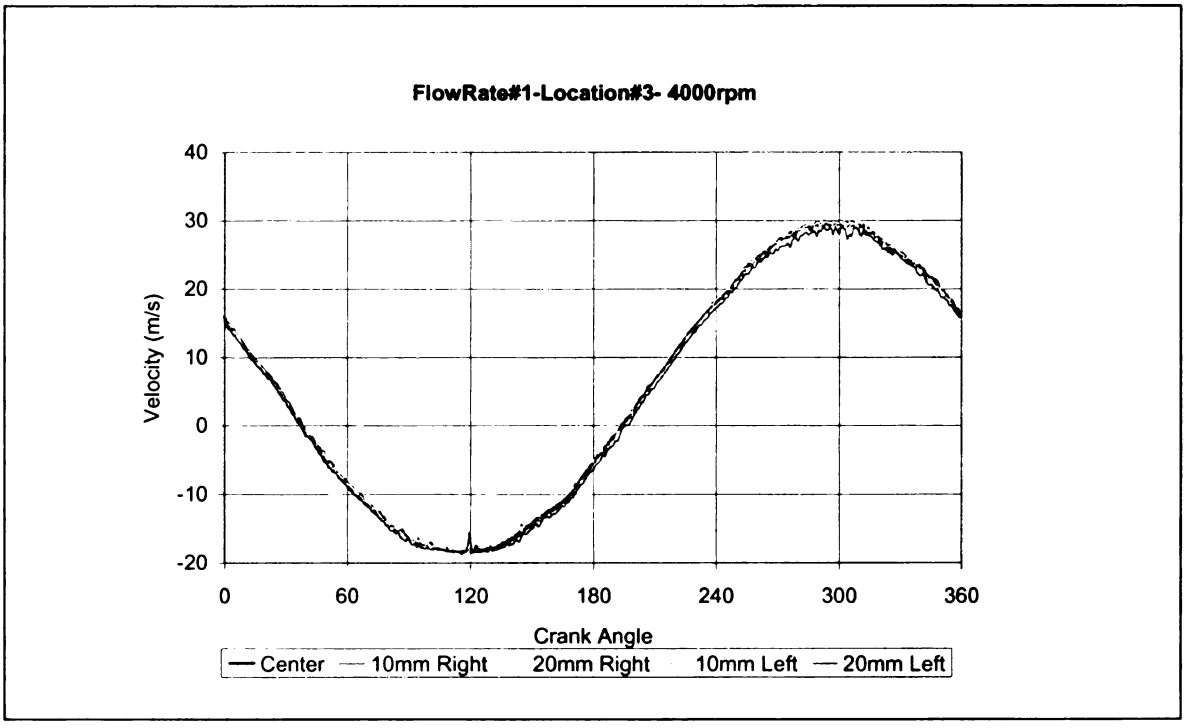

Figure 18: Velocity Profile at Location 3 (4000rpm, Flow Rate 1)

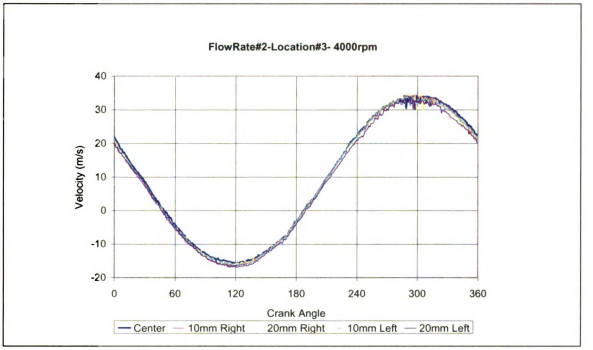

Figure 19: Velocity Profile at Location 3 (4000rpm, Flow Rate 2)

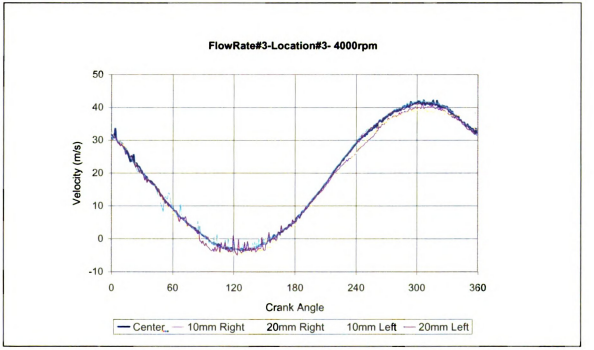

Figure 20: Velocity Profile at Location 3 (4000rpm, Flow Rate 3)

4.1.3 Discussion

When the results from three different locations are plotted in one plot, the velocity profiles for three different flow rates show a lot of similarities. In order to show the overall phenomenon, only the velocities in the center points were compared. Figure 21, Figure 22 and Figure 23 show the velocity results at the center of the cross section of the pipe for three different flow rates when the engine was running at 2000 rpm.

The three locations are near the piston, in the middle of the pipe and at the end of the pipe respectively.For all three plots, we can the velocities increase from the first location to the second location and decrease. This trend are shown in all the plots. The offset flow created by vacuum is the main reason for this. Without the vacuum, the flow is supposed to be up and down. With the vacuum, the flow is dragged backward when it is about to go up.

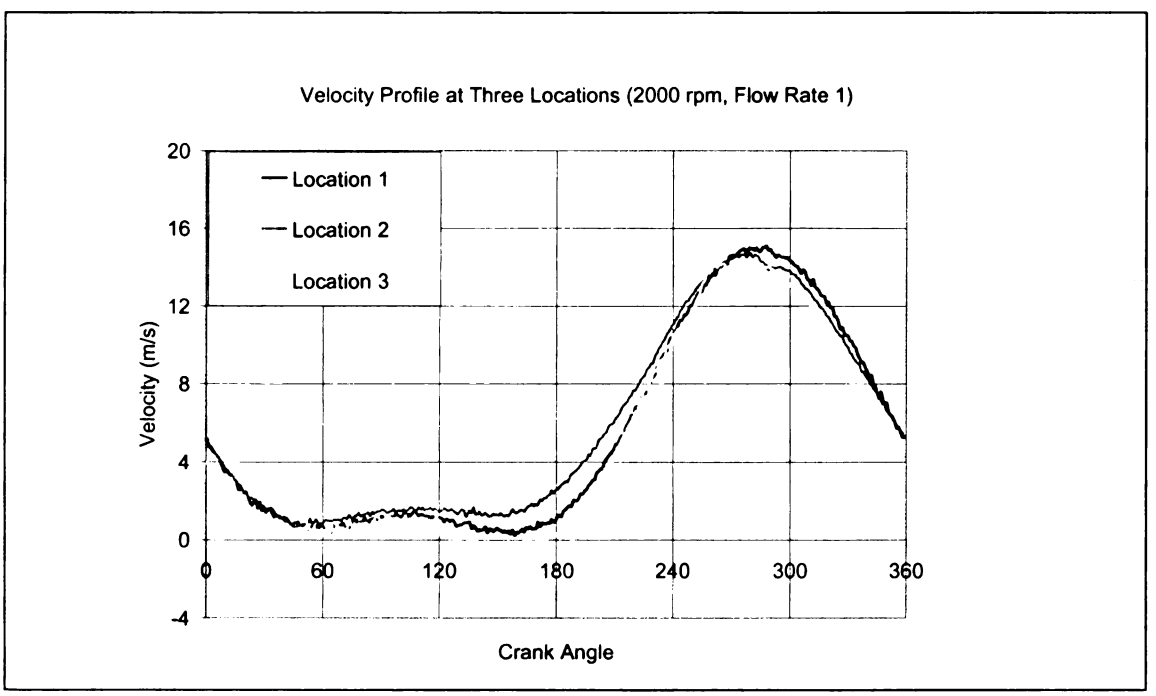

Figure 21: Velocity Profile at Three Locations (2000 rpm, Flow Rate 1)

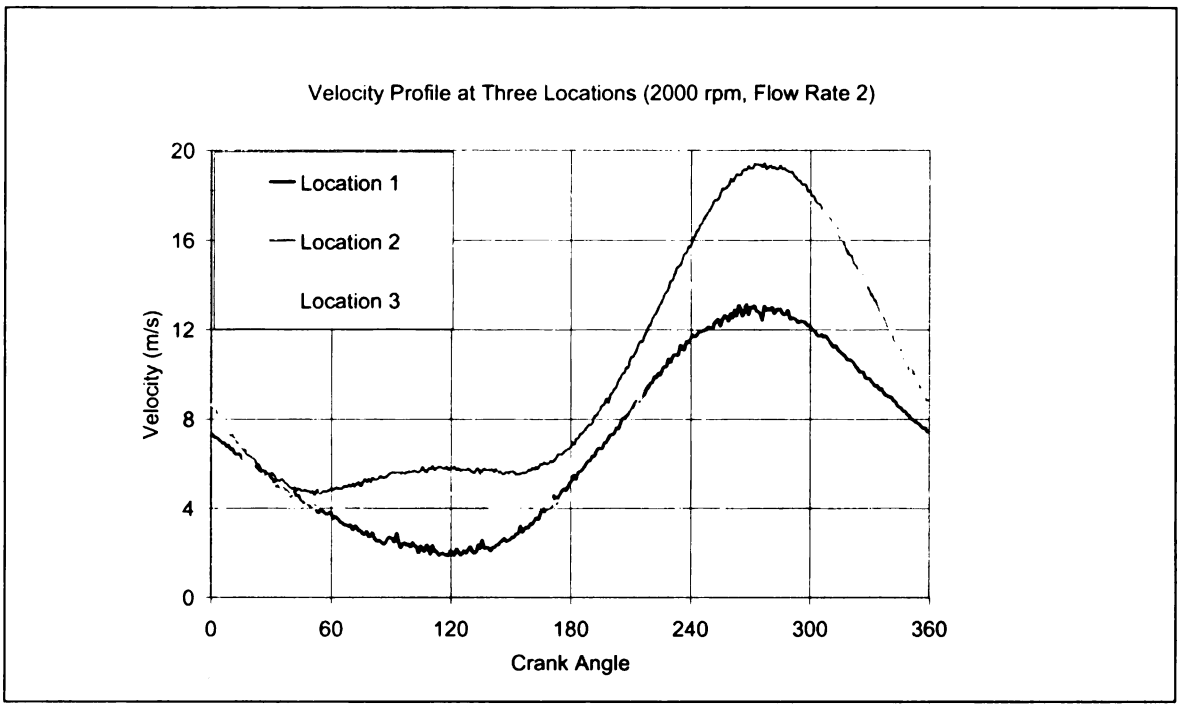

Figure 22: Velocity Profile at Three Locations (2000 rpm, Flow Rate 2)

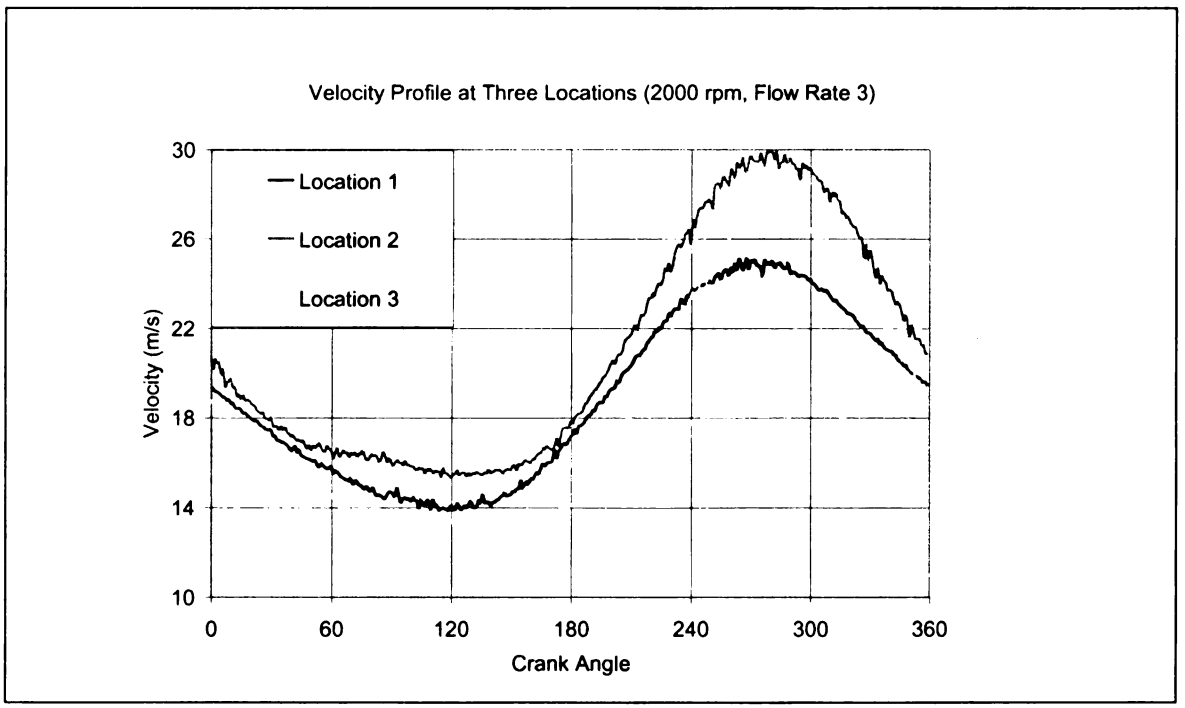

Figure 23: Velocity Profile at Three Locations (2000 rpm, Flow Rate 3)

4.2 Pressure Measurements

4.2.1 Pressure Measurements at 2000 rpm

Figure 24, Figure 25 and Figure 26 show the pressure drop at 2000 rpm at three different locations for three different flow rates. Although pressure measurements were only taken at three locations, it can show the pressure drop trend throughout the test region. Because the geometry is the straight pipe and the end of the pipe is always open to air at the atmosphere pressure.

The plot which shows pressure data vs. crank angles at each location is similar to the sine wave. The pressure starts at 14.7 psi, which is the atmosphere pressure.

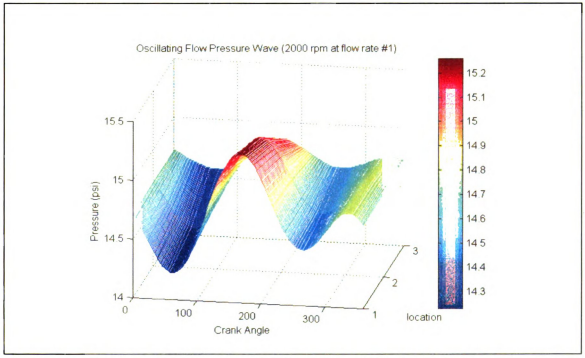

Figure 24: Pressure Drop at Three Different Locations (2000rpm, Flow Rate 1)

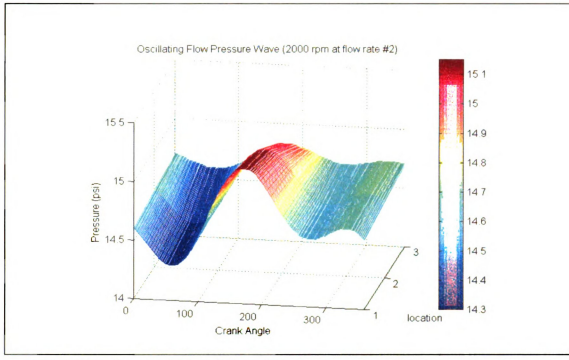

Figure 25: Pressure Drop at Three Different Locations (2000rpm, Flow Rate 2)

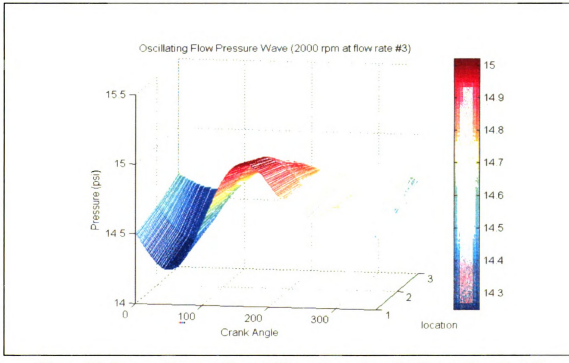

Figure 26: Pressure Drop at Three Different Locations (2000rpm, Flow Rate 3)

4.2.2 Pressure Measurements at 4000 rpm

Figure 27, Figure 28 and Figure 29 show the pressure drop at 4000 rpm at three different locations for three different flow rates.

Comparing to the results at 2000 rpm, the pressure magnitudes are larger and the curves of pressure data vs. crank angle at different locations are similar to the sine waves.

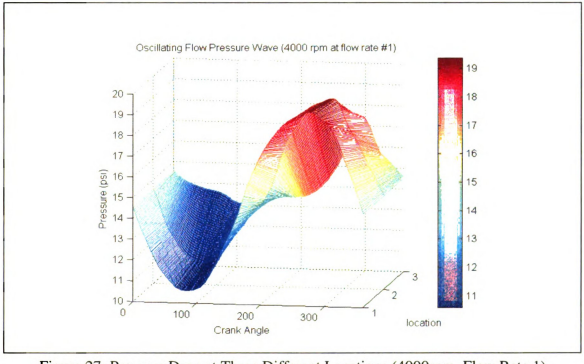

Figure 27: Pressure Drop at Three Different Locations (4000rpm, Flow Rate 1)

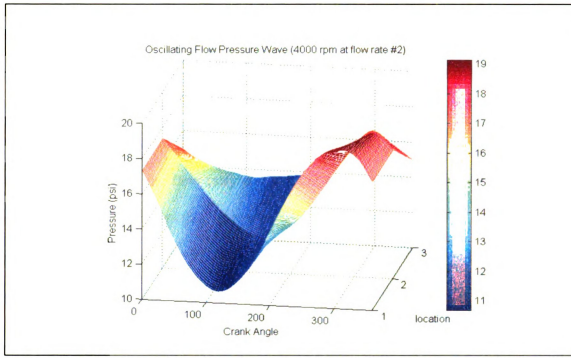

Figure 28: Pressure Drop at Three Different Locations (4000rpm, Flow Rate 2)

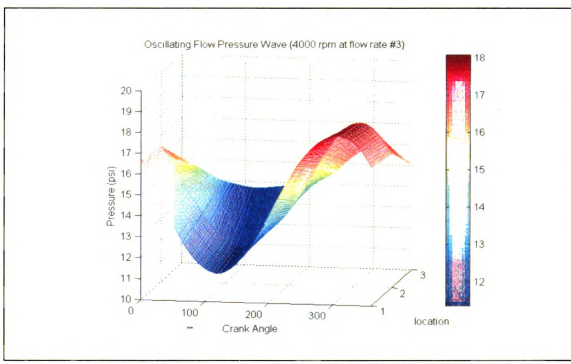

Figure 29: Pressure Drop at Three Different Locations (4000rpm, Flow Rate 3)

CHAPTER 5. NUMERICAL SIMULATION SETUP

5.1 Description of Problem

A schematic diagram of the problem investigated is shown in Figure 30. Basically, it involves the flow (air) in a straight pipe of round shape cross section with smooth walls. Because this problem is axisymmetric and the most important characteristics of the flow is the pressure and vertical velocity component, a two-dimensional analysis is used. The diagram shows the section selected for the simulation.

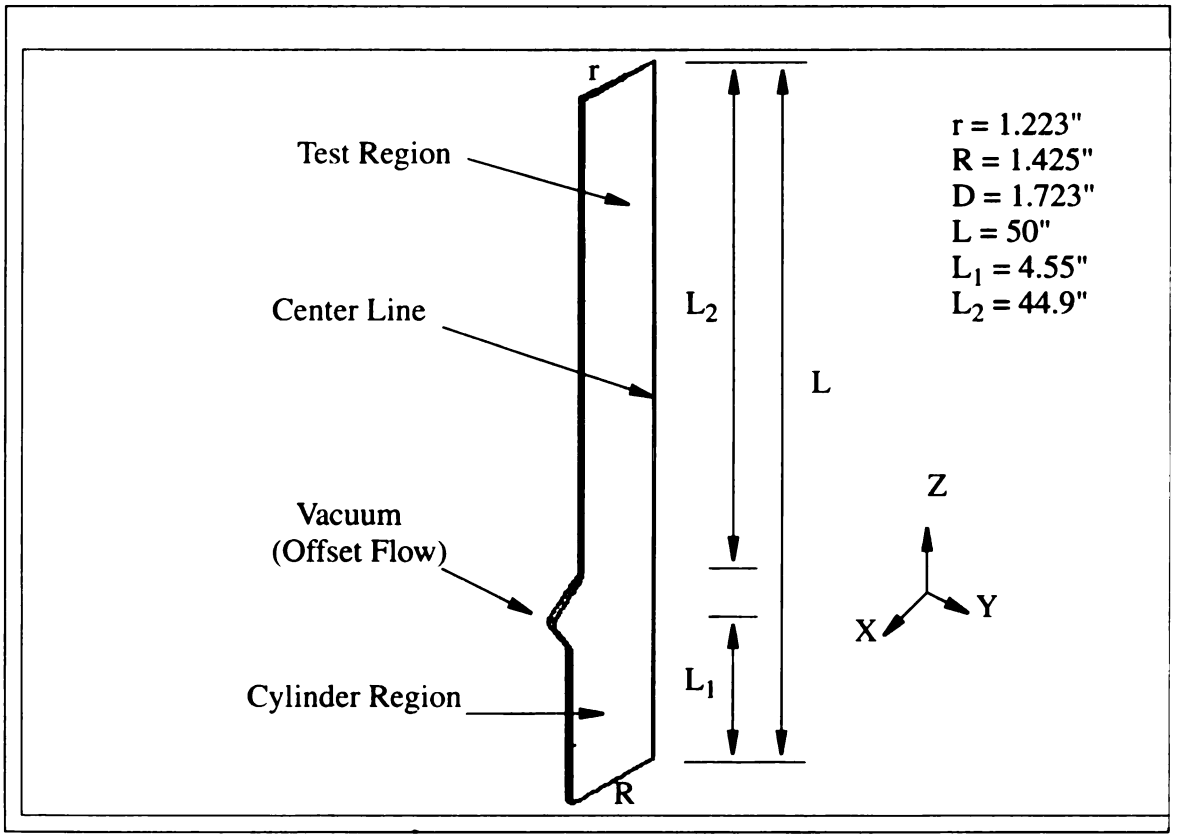

Figure 30: Schematic of Problem Studied

The simulation commences at bottom dead centre (BDC) and continues for a time interval corresponding to 360 of crank revolution. The fluid within the cylinder is assumed to be air, initially at room temperature and pressure. The flow is assumed to be turbulent and driven entirely by the motion of the piston and the pressure difference created by the vacuum. The pressures on the top of the pipe are held constant (at ambient conditions) throughout the simulation.

5.2 Formulation of Problem

5.2.1 Governing Equation

The governing equations for this problem were taken to be the ensemble-averaged conservation equations of mass (continuity), momentum (compressible Navier-Stokes), and total energy, closed by a high Reynolds number $\kappa - \varepsilon$ model.

$$\frac{\partial \rho}{\partial t} + \frac{\partial \rho u}{\partial x} + \frac{\partial \rho v}{\partial y} + \frac{\partial \rho w}{\partial z} = 0 \tag{1}$$

$$\frac{\partial}{\partial t}\begin{bmatrix} \rho u \\ \rho v \\ \rho w \end{bmatrix} + \frac{\partial}{\partial x}\begin{bmatrix} \rho uu \\ \rho vu \\ \rho wu \end{bmatrix} + \frac{\partial}{\partial y}\begin{bmatrix} \rho uv \\ \rho vv \\ \rho wv \end{bmatrix} + \frac{\partial}{\partial z}\begin{bmatrix} \rho uw \\ \rho vw \\ \rho ww \end{bmatrix} \tag{2}$$

$$= \frac{\partial}{\partial x}\begin{bmatrix} p^* + \tau_{xx} \\ \tau_{yx} \\ \tau_{zx} \end{bmatrix} + \frac{\partial}{\partial y}\begin{bmatrix} \tau_{xy} \\ p^* + \tau_{yy} \\ \tau_{zy} \end{bmatrix}$$

$$\frac{\partial e}{\partial t} + \frac{\partial}{\partial x}(e + p^*)u + \frac{\partial}{\partial y}(e + p^*)v + \frac{\partial}{\partial z}(e + p^*)w \tag{3}$$

$$= \frac{\partial}{\partial x}(\tau_{xx}u + \tau_{xy}v + \tau_{xz}w - q_x)$$

$$+ \frac{\partial}{\partial x}(\tau_{yx}u + \tau_{yy}v + \tau_{yz}w - q_y)$$

$$+ \frac{\partial}{\partial z}(\tau_{zx}u + \tau_{zy}v + \tau_{zz}w - q_z)$$

Where

$$P^* = P + \frac{2}{3}\rho k \tag{4}$$

5.2.2 Turbulent Model

The turbulent model used in this study is high Reynolds $k-\varepsilon$ model. It is the standard model, in which the high (turbulent) Reynolds number forms of the k and ε equations are used in conjunction with algebraic 'Law of the wall' representations of flow, heat and mass transfer for the near wall region. The initial turbulent kinematic energy and ε levels were defined before the simulation. The initialization of the turbulent intensity I at the inlet is 0.05 and the mixing length l is 0.0047 m (0.1D). Those quantities are used to calculate the initial TKE and ε levels.

$$k = 1.5 \times (U \times I)^2 \tag{5}$$

$$\varepsilon = C_\mu^{0.75} \times \frac{k^{1.5}}{l} \tag{6}$$

For this problem, the Reynold number is 2×10^5. The Reynold number was calculated at the main stream in the test region.

5.2.3 Boundary Conditions and Initial Conditions

The boundary and initial conditions for the governing equations and turbulent modes are as follows.

At the pipe inlet, the pressure an temperature as well as the turbulent quantities (turbulent intensity TI and mixing length l) were specified. The pressure was defined as the atmosphere pressure and the temperature was defined as the room temperature 293k.

At the pipe outlet, an average pressure was imposed for three different flow rates. At the walls of the pipe, the no-slip and adiabatic conditions were imposed.

There are three types boundary conditions defined in STAR-CD. The inlet and outlet were defined as the pressure boundaries. At the pipe inlet, i.e. at the top of the pipe, the pressure was defined as the atmosphere pressure and the turbulence quantities were specified. At the pipe outlet, i.e. where the offset flow passed through, the vacuum pressures were defined for three different flow rates. The vacuum pressures were -4 kpa, -20 kpa and -40 kpa respectively (all relative to atmosphere pressure).The symmetry boundaries were defined to reduce the size of the computational mesh by placing the boundary along the planes of geometrical and flow symmetry. The pipe surface and the cylinder surface are defined as the wall boundaries. The wall was set to 'no slip' and adiabatic. The wall roughness was set to be standard.

The initial conditions of this transient problem are: room temperature and pressure. The piston starts from the BDC. At the last step of each run, the results were written into a restart file. Then for the next run, the analysis starts from the restart file.

5.3 Numerical Method of Solution

5.3.1 Introduction to STAR-CD

Solutions to the government equations described in the previous section were obtained by using the STAR-CD version 3.10, developed by Analysis and Design Applications Company, Ltd. STAR-CD is one of the leading multi-purpose thermofluids analysis codes. It is designed for engineers and scientists requiring a versatile, efficient and robust software package capable of modeling fluid flow, heat transfer, mass transfer and chemical reaction in industry and the environment.

STAR-CD is a self-contained package incorporating: mathematical models of a wide range of thermofluids phenomena, powerful solvers enabling full complex-geometry capabilities and flexible pre-processing and post-processing facilities tailored for both expert and novice users. The code can also be readily integrated with other computer-aided engineering software for any of the following functions: surface modeling, mesh generation, mesh and results display and provision of STAR boundary information to structural analysis codes. This is achieved by internal translators between the STAR-CD and external file formats, including PATRAN, IDEAS, ANSYS, GRID3D, NASTRAN, STL AND IGES. STAR-CD has been ported to a wide range of computers comprising PCs, workstations, minicomputers, mainframe machines and super computers. Optimized versions have also been developed for vector, parallel and vector/parallel architectures.

5.3.2 Solution Algorithm

STAR-CD currently incorporates three different implicit algorithms, namely: SIMPLE, PISO and SIMPISO. Since PISO is applicable to both transient and steady-state calculations and is particularly suitable for the former, for which it has been shown to be considerably more efficient than iterative methods, PISO was chosen as the algorithm used in this study.

PISO performs at each time (or iteration) step, a predictor, followed by a number of correctors, during which linear equation sets are solved iteratively for each main dependent variable. The decisions on the number of correctors and inner iterations (hereafter referred to as 'sweeps', to avoid confusion with outer iterations performed as part of the steady-state solution mode) are made internally on the basis of the splitting error and inner residual levels, respectively, according to prescribed tolerances and upper

limits. The default values for the solver tolerances and maximum correctors and sweeps are given in Table 4.

Table 4: Standard Control Parameter Settings for Transient PISO Calculations

Parameter	Variable				
	Velocity	Pressure	Turbulence	Enthalpy	Concentration
Solver tolerance	0.01	0.001	0.01	0.01	0.01
Sweep limit	100	1000	100	100	100
Correction limit = 20					
Pressure correction relaxation factor = 1.0					
Corrector step tolerance = 0.25					

The remaining key parameter in transient calculations with PISO is the size of the time increment δt. This is normally determined by accuracy considerations and may be varied during the course of the calculation. The step should ideally be of the same order of magnitude as the smallest characteristic time δt_c for convection and diffusion, i.e.

$$\delta t_c = min\left(\frac{\delta L}{U}, \frac{\rho \delta L^2}{\Gamma}\right) \tag{7}$$

Here, U and Γ are a characteristic velocity and diffusivity, respectively, and δL is a mean mesh dimension. Typically, it is possible to operate with $\delta t = 50\ \delta t_c$ and still obtain reasonable temporal accuracy. Values significantly above this may lead to errors and numerical instability, whereas smaller values will lead to increased computing times.

During the course of a calculation, the limits given in Table 4 may be reached, in which case messages to this effect will be produced. This is most likely to occur during

the start-up phase but is nevertheless acceptable if, later on, the warnings either cease entirely or only appear occasionally, and the predictions look reasonable. If, however, the warnings persist, corrective actions should be taken. The possible actions are: reduction in time step, increasing in the sweep limits, changing the value of pressure correction under-relaxation, or setting the corrector step tolerance to a lower value.

5.3.3 Grid System Used

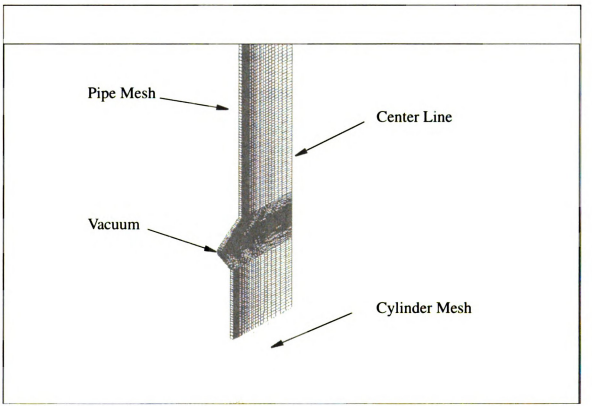

Figure 31: Grid System Used

The domain of the problem was replaced by a single-block grid system that was assembled by patching together two blocks of structured grids. It is shown in Figure 31. The two blocks are cylinder mesh and the pipe mesh in the test region. The total

number of defined cells is 30654. The mesh was created by Gridgen. Gridgen is a software system for the generation of 3D grids.

5.3.4 Solution Procedures

Firstly, run the problem without piston movement and observe the streamlines in the duct, especially the velocity profile in the orifice.

Then close the vacuum part and set boundary and initial conditions as previously discussed and run the first cycle. Then run the simulation several cycles until the periodical results were achieved.

After that, open the vacuum part and slowly decrease the vacuum pressure to run the problem under different flow rates. For each case, several runs were needed to reach the periodical results.

CHAPTER 6. NUMERICAL SIMULATION RESULTS AND DISSCUTION

6.1 Velocity Results

6.1.1 Velocity Profile for Different Flow Rates at 2000 rpm

From Figure 32 to Figure 37, velocity profiles at 2000 rpm at three different locations and three different flow rates are shown. Since the volume of post data files are huge, only the cells at the same locations were investigated. The velocity profiles were plotted vs. crank angle at 20 degree interval. The comparison to the experimental results will be discussed in the next chapter.

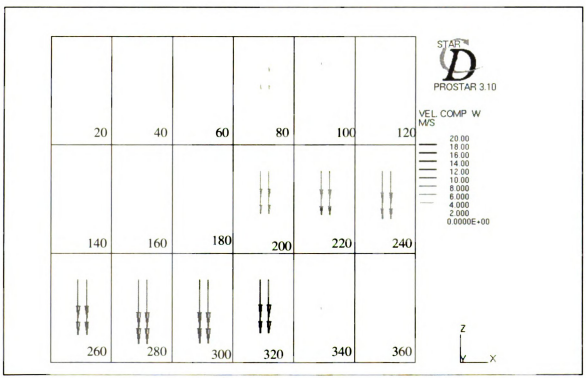

Figure 32: Velocity Profile at Location 1 (2000rpm, Flow Rate 1)

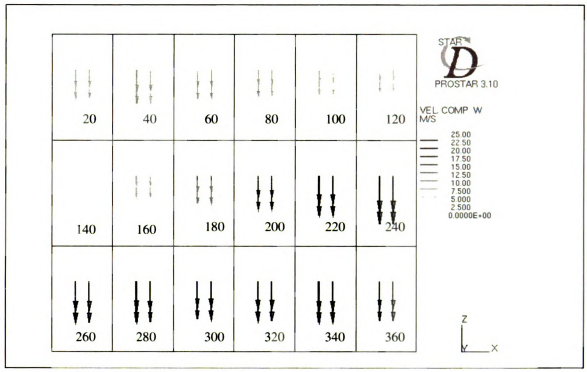

Figure 33: Velocity Profile at Location 2 (2000rpm, Flow Rate 2)

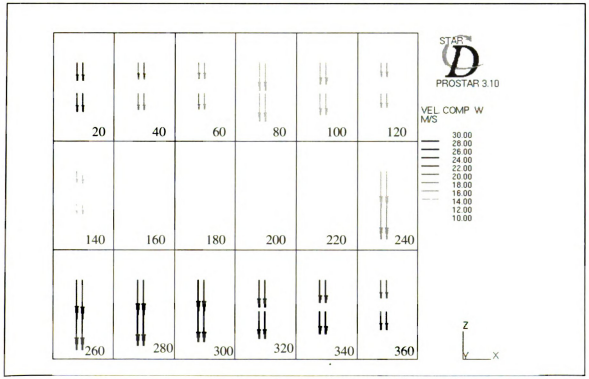

Figure 34: Velocity Profile at Location 3 (2000rpm, Flow Rate 3)

6.1.2 Velocity Profile for Different Flow Rates at 4000 rpm

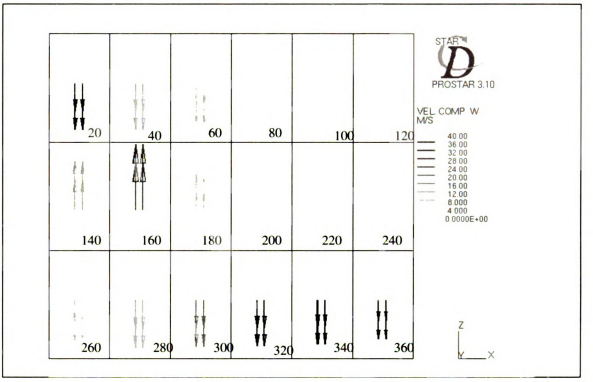

Figure 35: Velocity Profile at Location 1 (4000rpm, Flow Rate 1)

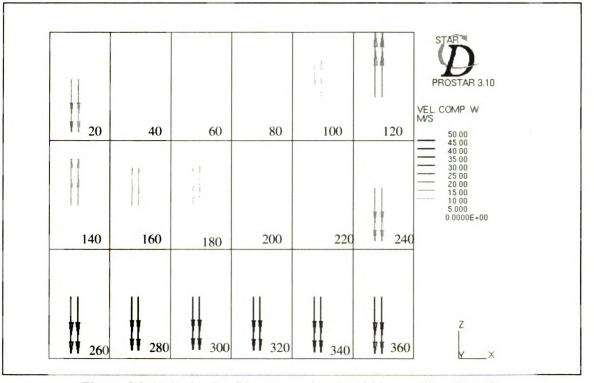

Figure 36: Velocity Profile at Location 2 (4000rpm, Flow Rate 2)

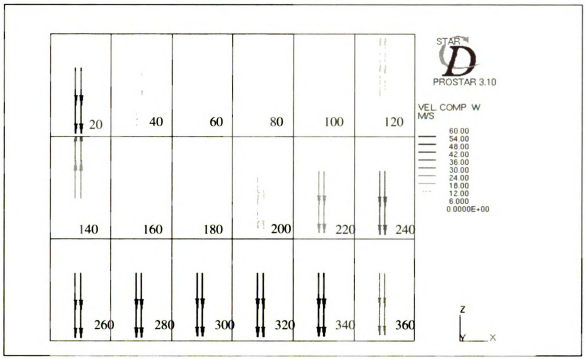

Figure 37: Velocity Profile at Location 3 (4000rpm, Flow Rate 3)

6.1.3 Velocity profiles in the region of orifice (outlet of the pipe)

The velocity profiles in the region of the orifice are affected by both piston movement and the vacuum pressure difference. It is important to show the flow patterns in this region. Because the profiles in this region will influence the results in the upstream calculations.

From Figure 38 to Figure 43, the velocity profiles near the region of orifice with function of the crank angle are shown, when engine was running at 2000 rpm and flow rate 1, i.e. the vacuum pressure was set at 4kpa below the atmosphere pressure.

From Figure 44 to Figure 49, the velocity profiles near the region of orifice with function of the crank angle are shown, when engine was running at 2000 rpm and flow rate 1.

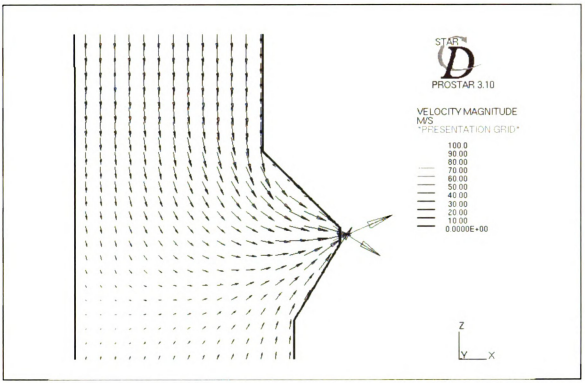

Figure 38: Velocity Profile in the Region of Orifice at 2000 rpm (CA=60)

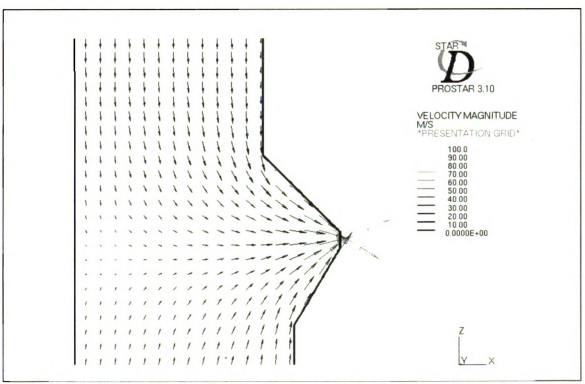

Figure 39: Velocity Profile in the Region of Orifice at 2000 rpm (CA=120)

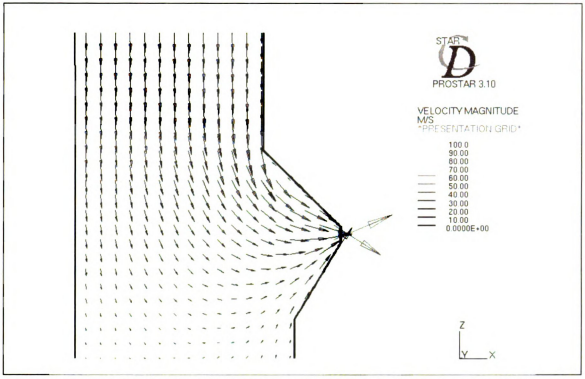

Figure 40: Velocity Profile in the Region of Orifice at 2000 rpm (CA=180)

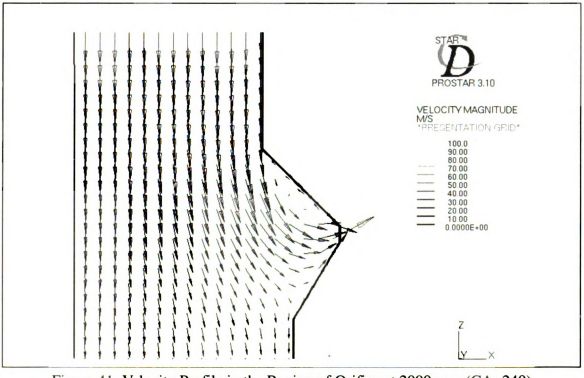

Figure 41: Velocity Profile in the Region of Orifice at 2000 rpm (CA=240)

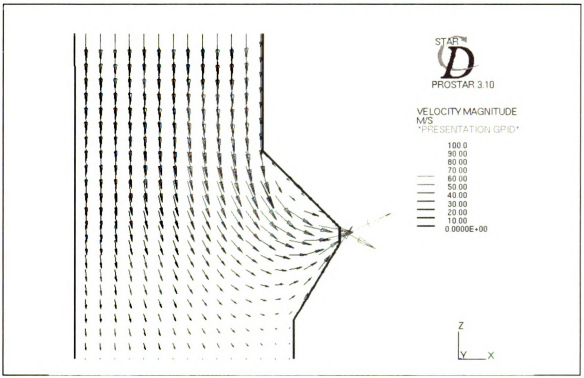

Figure 42: Velocity Profile in the Region of Orifice at 2000 rpm (CA=300)

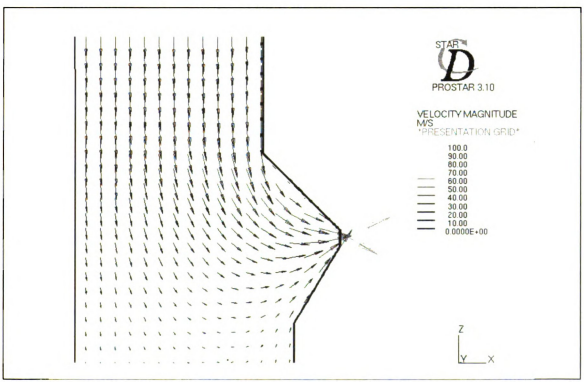

Figure 43: Velocity Profile in the Region of Orifice at 2000 rpm (CA=360)

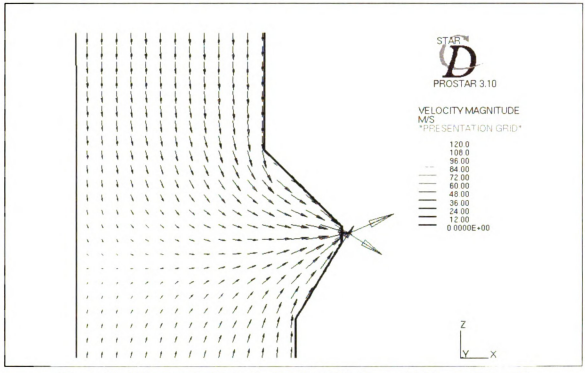

Figure 44: Velocity Profile in the Region of Orifice at 4000 rpm (CA=60)

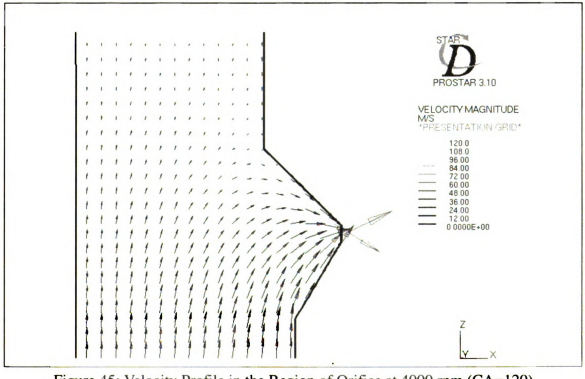

Figure 45: Velocity Profile in the Region of Orifice at 4000 rpm (CA=120)

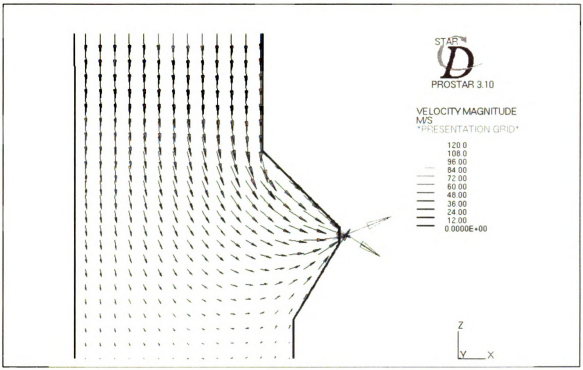

Figure 46: Velocity Profile in the Region of Orifice at 4000 rpm (CA=180)

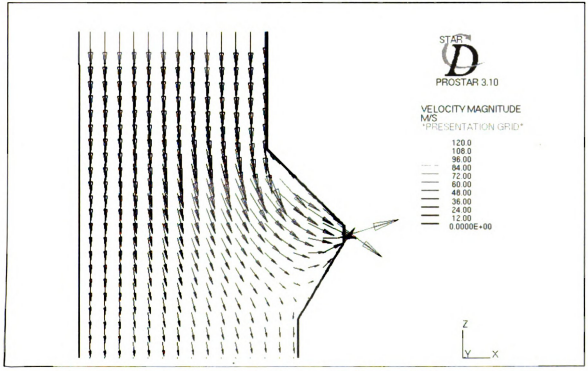

Figure 47: Velocity Profile in the Region of Orifice at 4000 rpm (CA=240)

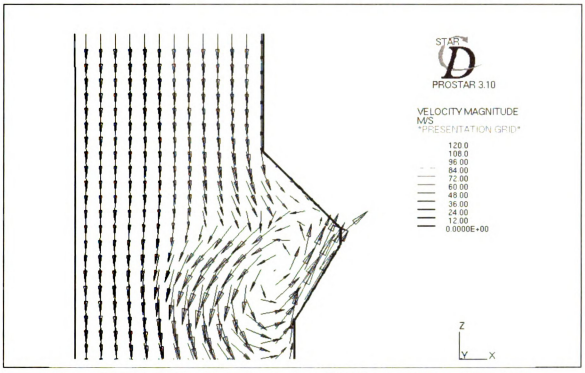

Figure 48: Velocity Profile in the Region of Orifice at 4000 rpm (CA=300)

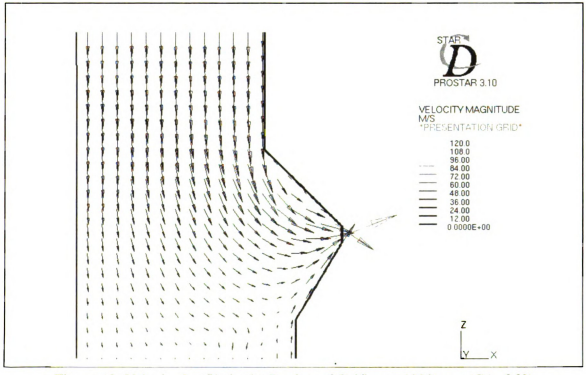

Figure 49: Velocity Profile in the Region of Orifice at 4000 rpm (CA=360)

In Figure 49, there is a vertex near the orifice. The reason for this is the influences of the piston movements and the vacuum pressure. Since the velocities in the pipe reach to the maximum values at about 300 crank angle, the drag force created by the piston plays an important role. Also, comparing the velocity profiles in the region of orifice between 2000 rpm and 4000 rpm, the piston movement plays a more important role in the latter one.

6.2 Pressure Results

6.2.1 Pressure Results for 2000 rpm.

From Figure 50 to Figure 55 the pressure wave development in the first cycle are shown when engine is running at 2000 rpm.

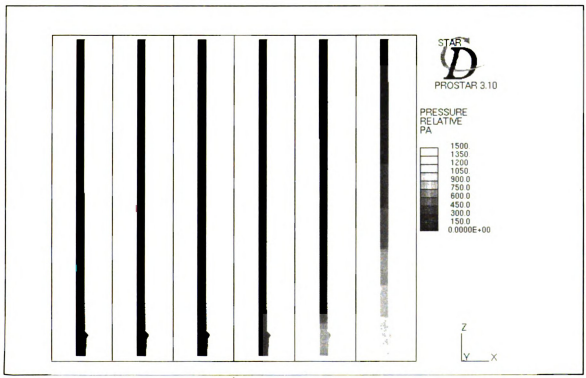

Figure 50: Pressure Results for Crank Angle 10 - 60 Degree (2000 rpm)

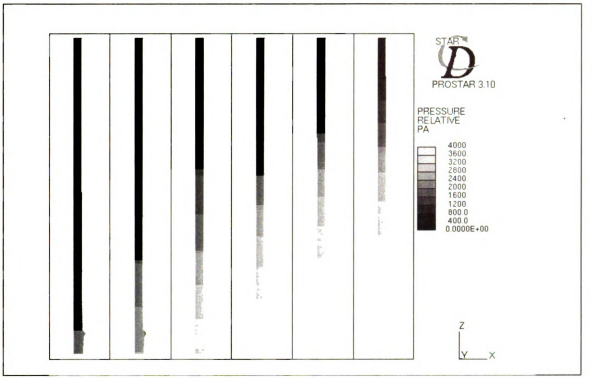

Figure 51: Pressure Results for Crank Angle 70 - 120 Degree (2000 rpm)

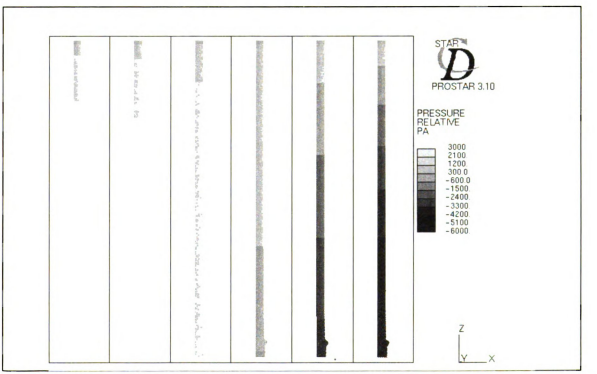

Figure 52: Pressure Results for Crank Angle 130 - 180 Degree (2000 rpm)

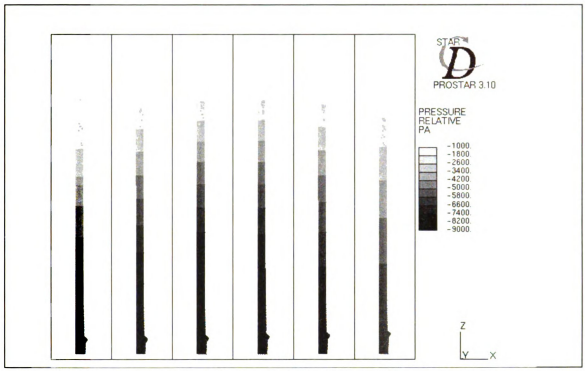

Figure 53: Pressure Results for Crank Angle 190 - 240 Degree (2000 rpm)

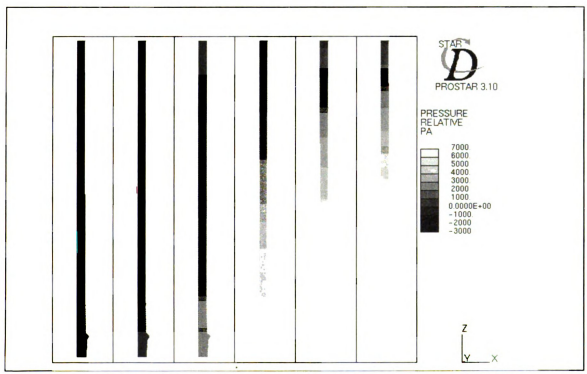

Figure 54: Pressure Results for Crank Angle 250 - 300 Degree (2000 rpm)

Figure 55: Pressure Results for Crank Angle 310 - 360 Degree (2000 rpm)

From Figure 50 to Figure 55, we can see how the pressure wave developed in the first cycle. This can be demonstrated easily by the numerical simulation. On the contrary, it is very difficult for the experimental approach to be applied when the engine just turned on.

6.2.2 Pressure Results for 4000 rpm

From Figure 56 to Figure 61 the pressure wave development in the first cycle are shown when engine is running at 4000 rpm.

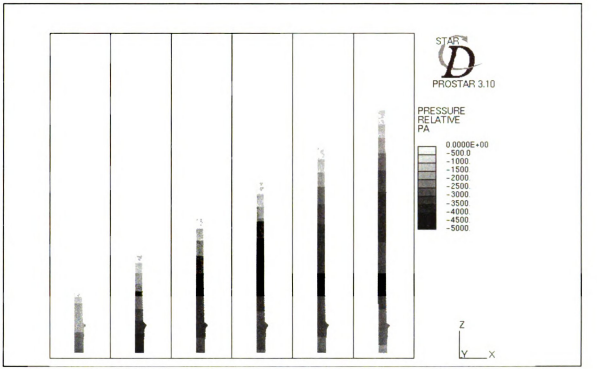

Figure 56: Pressure Results for Crank Angle 10 - 60 Degree (4000 rpm)

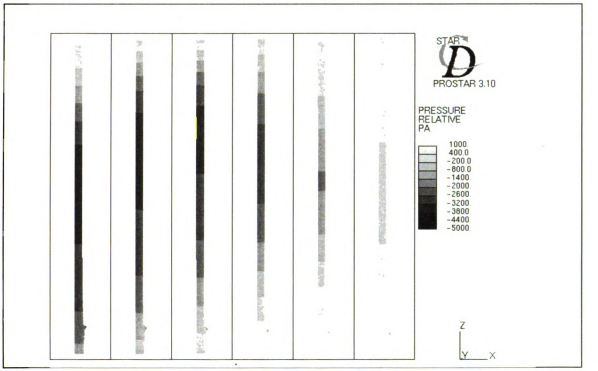

Figure 57: Pressure Results for Crank Angle 70 - 120 Degree (4000 rpm)

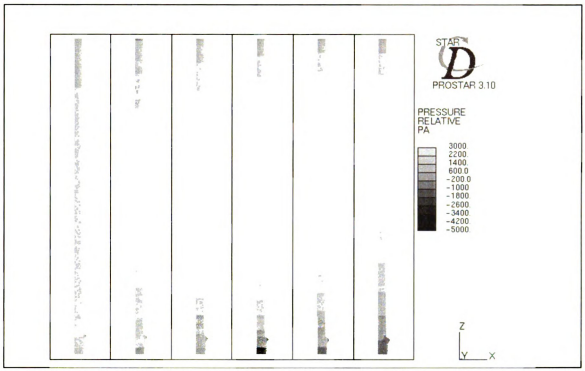

Figure 58: Pressure Results for Crank Angle 130 - 180 Degree (4000 rpm)

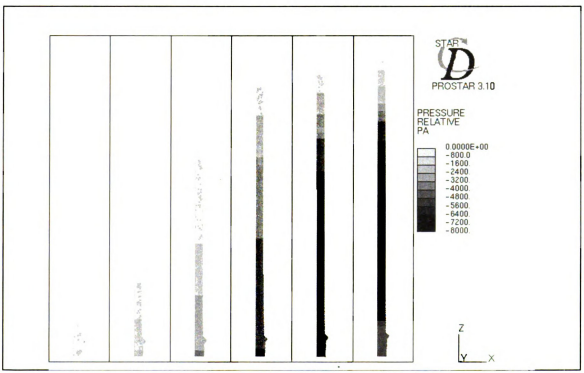

Figure 59: Pressure Results for Crank Angle 190 - 240 Degree (4000 rpm)

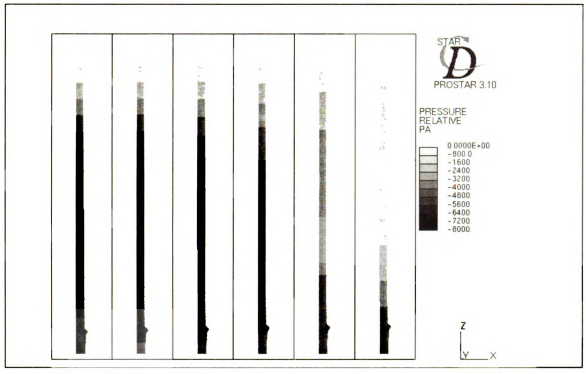

Figure 60: Pressure Results for Crank Angle 250 - 300 Degree (4000 rpm)

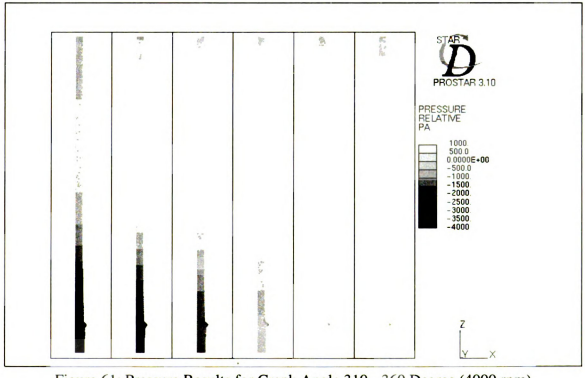

Figure 61: Pressure Results for Crank Angle 310 - 360 Degree (4000 rpm)

The periodical results at the same locations where the measurements were taken will be compared in the next chapter.

CHAPTER 7. COMPARISON

7.1 Compare the CFD Velocity Results with LDV Results.

7.1.1 Comparison at 2000 rpm

From the vast amount of data from the simulation, only a few major findings are discussed in this chapter. In order to compare the results of simulation and LDV, we should choose the cell or cells in the grid at the same location and the comparison must be in the same conditions, i.e. same engine speed and flow rate. All velocity results are plotted as the function of the crank angle. The three locations are 12 inches, 25inches and 43inches from the piston top surface. Since the post data files in STAR-CD recorded data every 10 crank angle degrees, the results from CFD in the figures are plotted every 10 crank angle degrees. Because the size of the post file would be huge if the data were saved during the simulations for every crank angle during the runs.

From Figure 62 to Figure 64, the comparisons are shown at the first flow rate. At all three locations, the predicted and experimental results show the same trend lines. There is a phase lag between two plots in each figure. It is about 30 to 40 degree. The largest discrepancy is between 30 and 120 crank angle when piston moves from BDC to TDC in Figure 63. The predicted results are almost twice as the measured ones. The velocity magnitude differences between two results for all three figures are less than 10 percent for the maximum values. The velocity magnitude differences between two results for all three figures are about 50 percent for the minimum values.

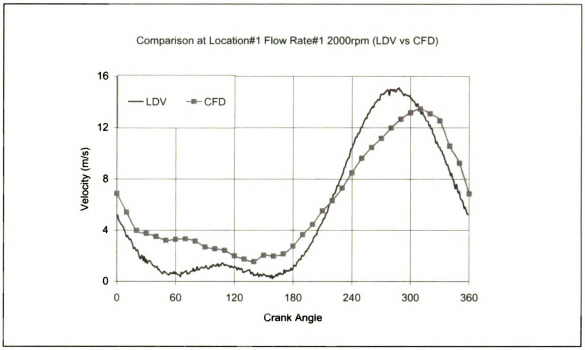

Figure 62: Velocity Profile Comparison at 2000 rpm (Location 1, Flow Rate 1)

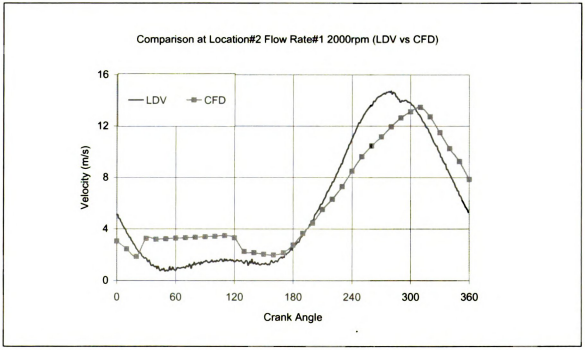

Figure 63: Velocity Profile Comparison at 2000 rpm (Location2, Flow Rate 1)

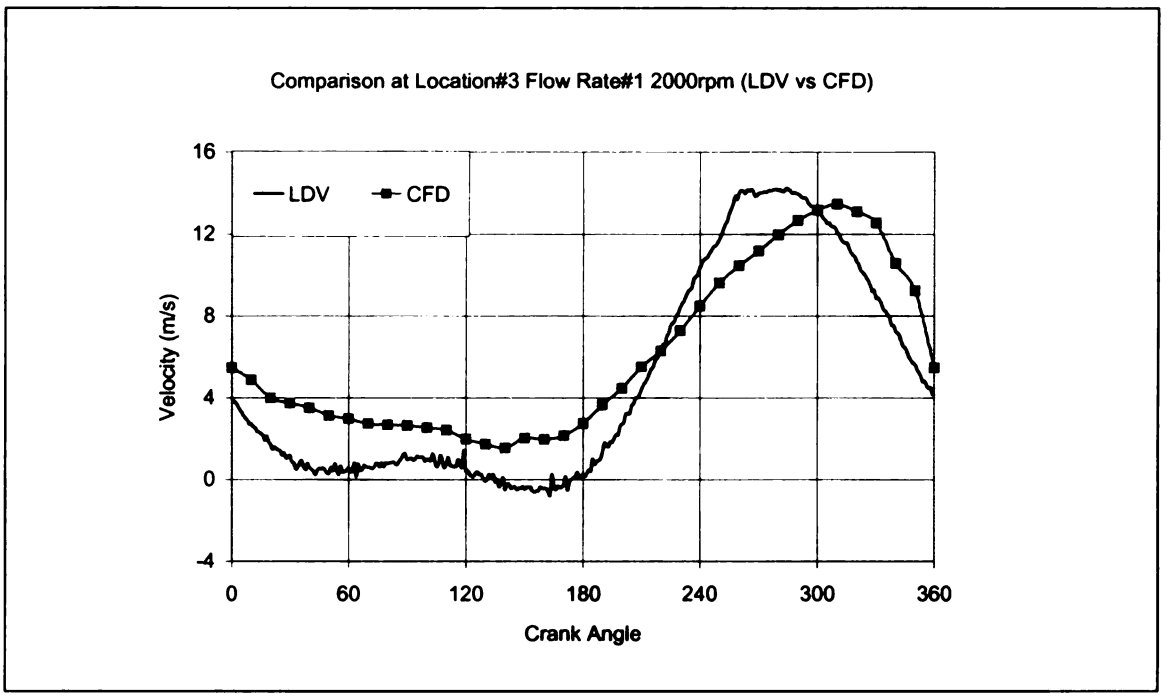

Figure 64: Velocity Profile Comparison at 2000 rpm (Location 3, Flow Rate 1)

From Figure 65 to Figure 67, the comparisons are shown at the second flow rate. In all three figures, the predicted and experimental results show the same trend lines. There is a phase lag between two plots at location 1 and 3. It is about 30 to 40 degree. The velocity magnitude differences between two results for all three figures are less than 10 percent for the maximum values in location 1 and 3. For location 2, the difference is about 30 percent. The velocity magnitude differences between two results for all three figures are about 40 percent for the maximum values for location 2 and 3.

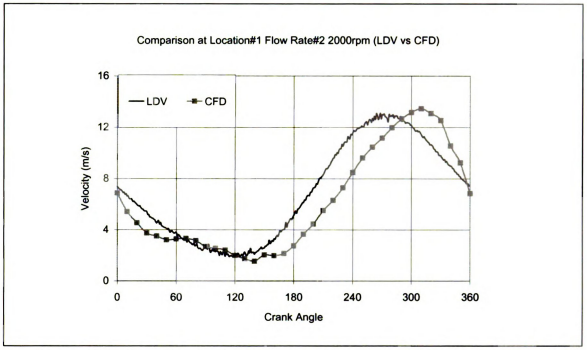

Figure 65: Velocity Profile Comparison at 2000 rpm (Location 1, Flow Rate 2)

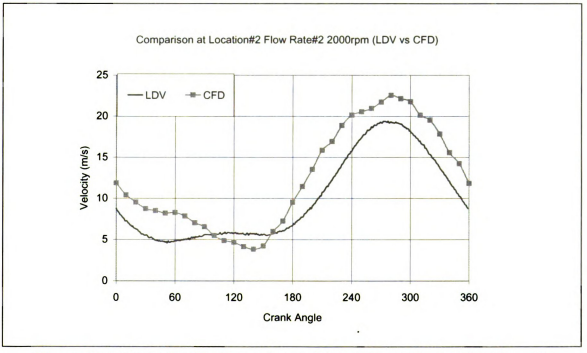

Figure 66: Velocity Profile Comparison at 2000 rpm (Location 2, Flow Rate 2)

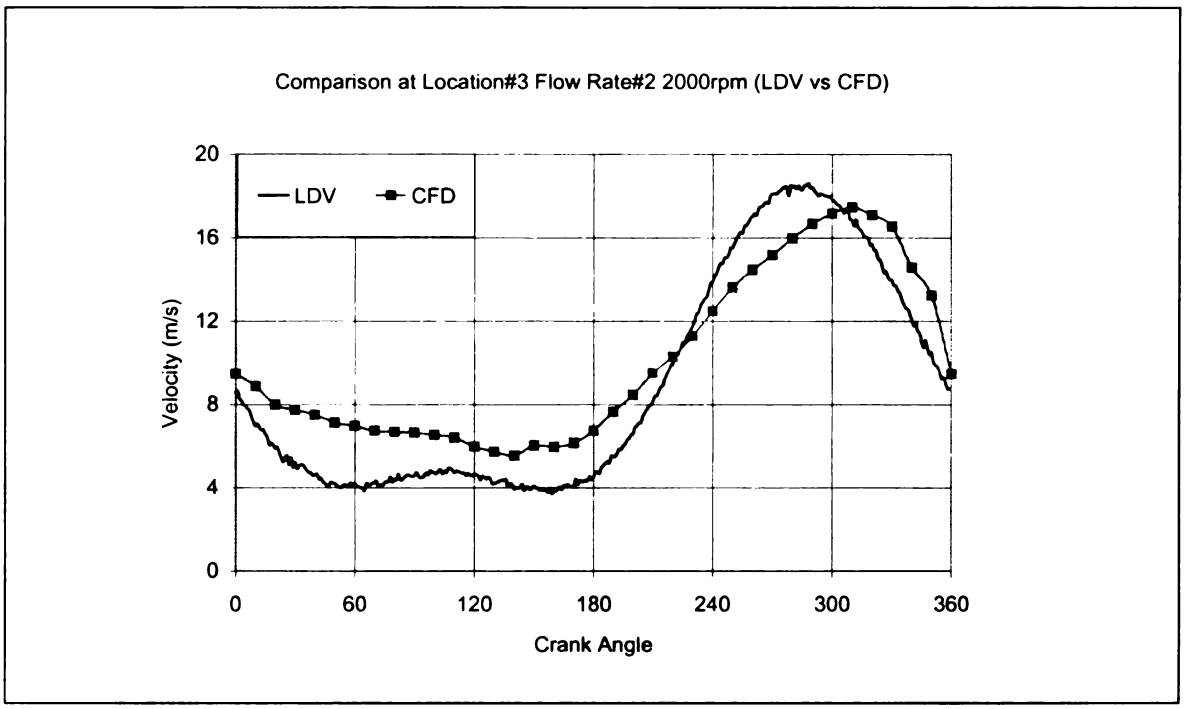

Figure 67: Velocity Profile Comparison at 2000 rpm (Location 3, Flow Rate 2)

From Figure 68 to Figure 70, the comparisons are shown at the third flow rate. The velocity magnitudes for this one are much larger than the previous two flow rates. In all three figures, the predicted and experimental results show the same trend lines. There is also a phase delay between two plots at all locations. It is about 40 degree.

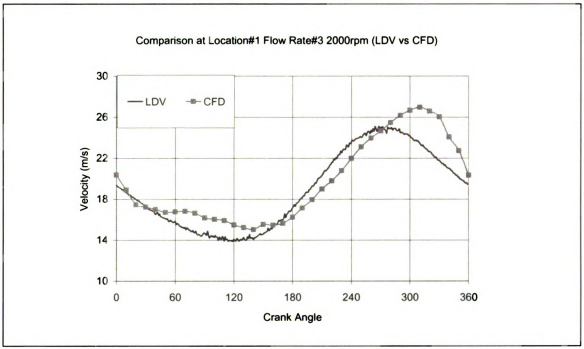

Figure 68: Velocity Profile Comparison at 2000 rpm (Location 1, Flow Rate 3)

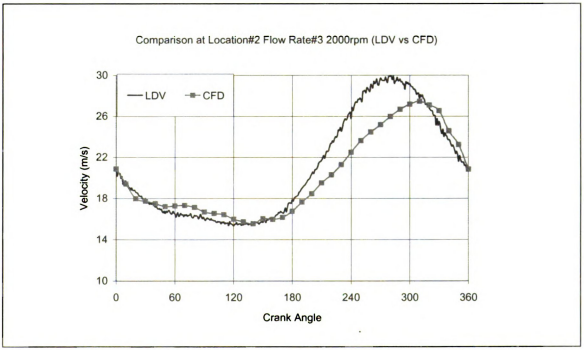

Figure 69: Velocity Profile Comparison at 2000 rpm (Location 2, Flow Rate 3)

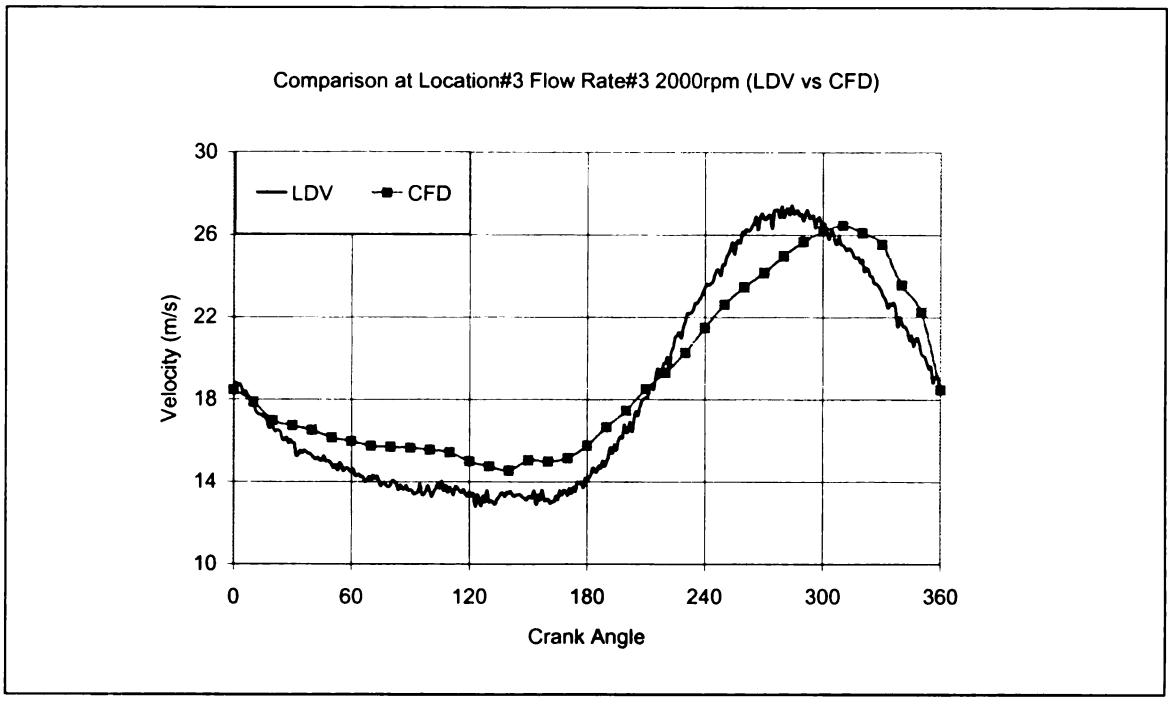

Figure 70: Velocity Profile Comparison at 2000 rpm (Location 3, Flow Rate 3)

7.1.2 Comparison at 4000 rpm

From Figure 71 to Figure 76, the comparisons are shown at 4000 rpm at two different locations (location 2 and location 3) and at three different flow rates.

In all six figures, the predicted and experimental results show the same trend lines. In Figure 75 and 76, the predicted results show some negative values between 60 and 180 degree. That means the velocity direction is away from the piston.

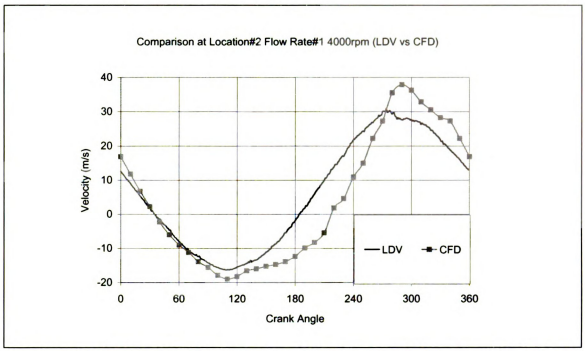

Figure 71: Velocity Profile Comparison at 4000 rpm (Location 2, Flow Rate 1)

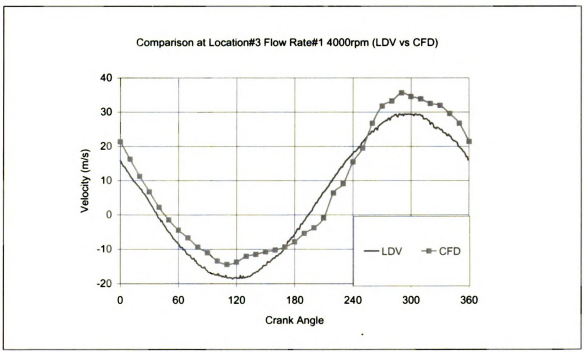

Figure 72: Velocity Profile Comparison at 4000 rpm (Location 3, Flow Rate 1)

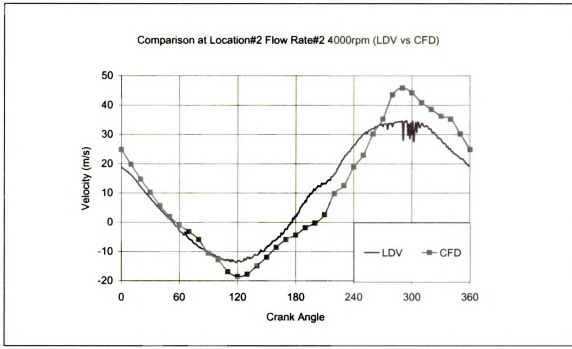

Figure 73: Velocity Profile Comparison at 4000 rpm (Location 2, Flow Rate 2)

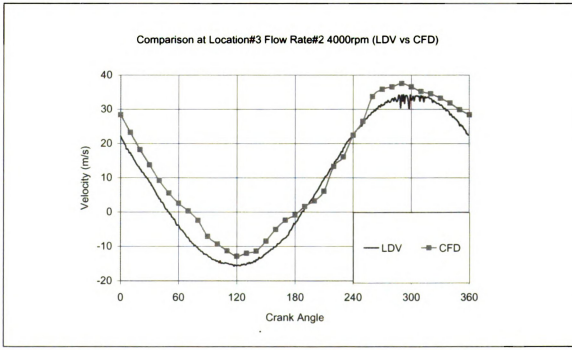

Figure 74: Velocity Profile Comparison at 4000 rpm (Location 3, Flow Rate 2)

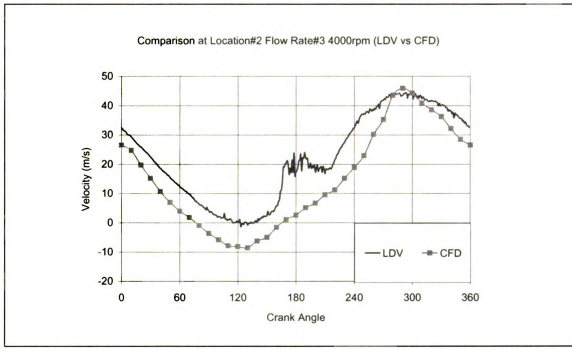

Figure 75: Velocity Profile Comparison at 4000 rpm (Location 2, Flow Rate 3)

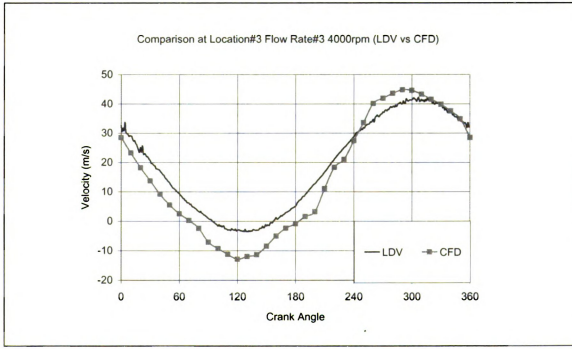

Figure 76: Velocity Profile Comparison at 4000 rpm (Location 3, Flow Rate 3)

7.2 Compare the CFD Pressure Results with Experimental Results

7.2.1 Comparison at 2000 rpm

The results' unit from the pressure transducer measurements was changed from pa to psi and then compared to the CFD in this section. The comparisons at 2000 rpm are shown from Figure 77 to Figure 85. The simulation results are compared with experimental data at every location and at each flow rate.

All the comparisons at 2000 rpm show the same trend lines. All the pressure waves have the similar shape to the letter w. The differences between the measured and predicted pressure data are all less than 10 percent, which is much better than the comparisons of the velocity.

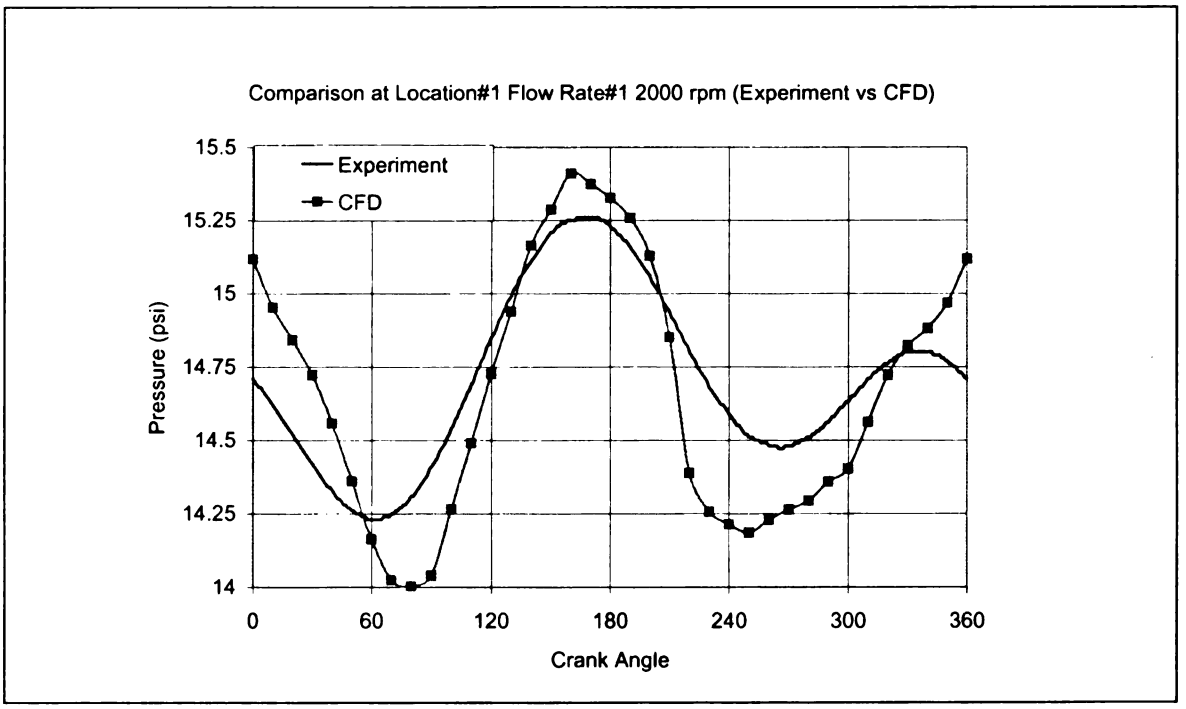

Figure 77: Pressure Data Comparison at 2000 rpm (Location 1, Flow Rate 1)

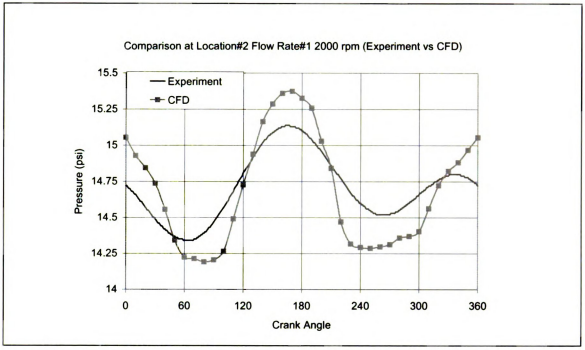

Figure 78: Pressure Data Comparison at 2000 rpm (Location 2, Flow Rate 1)

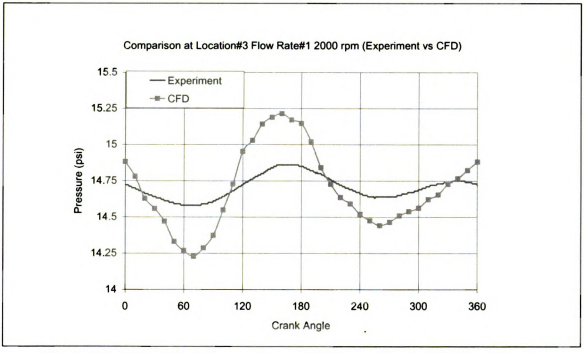

Figure 79: Pressure Data Comparison at 2000 rpm (Location 3, Flow Rate 1)

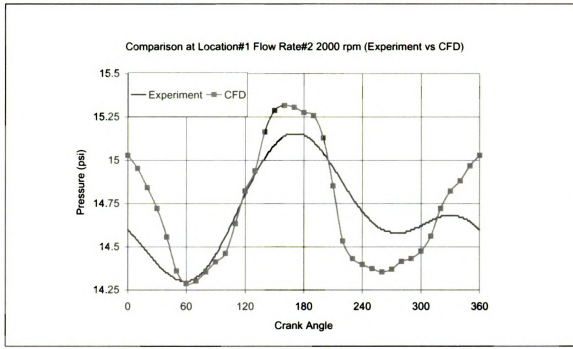

Figure 80: Pressure Data Comparison at 2000 rpm (Location 1, Flow Rate 2)

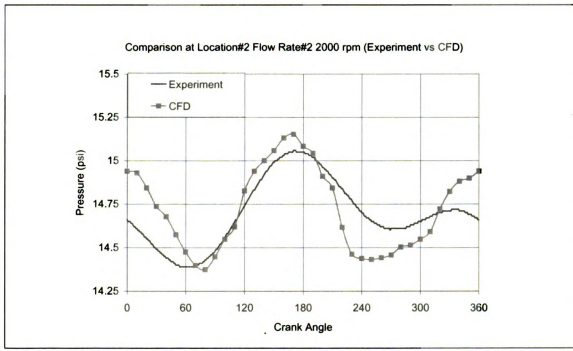

Figure 81: Pressure Data Comparison at 2000 rpm (Location 2, Flow Rate 2)

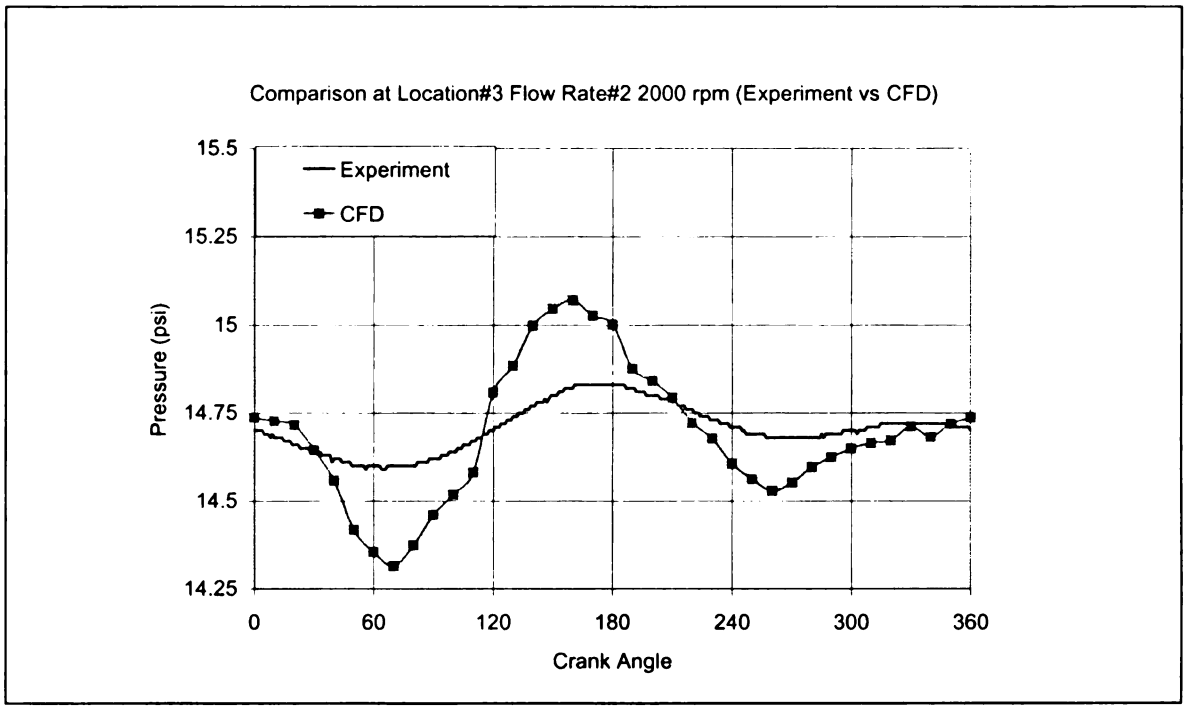

Figure 82: Pressure Data Comparison at 2000 rpm (Location 3, Flow Rate 2)

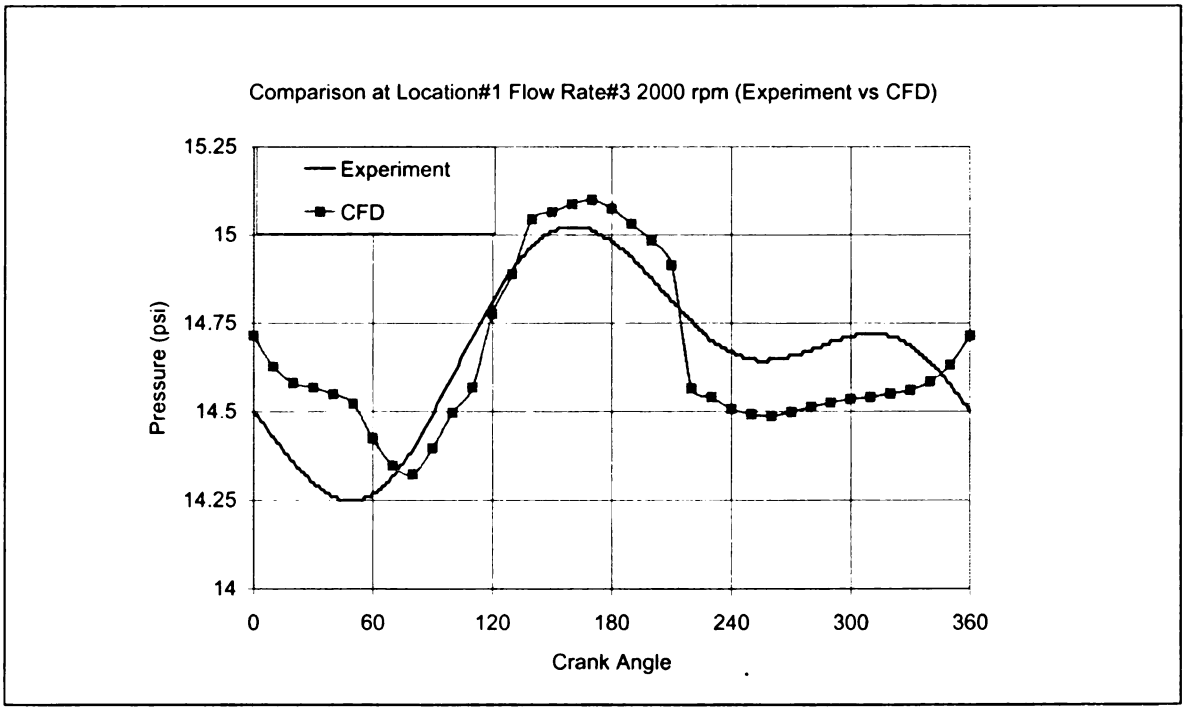

Figure 83: Pressure Data Comparison at 2000 rpm (Location 1, Flow Rate 3)

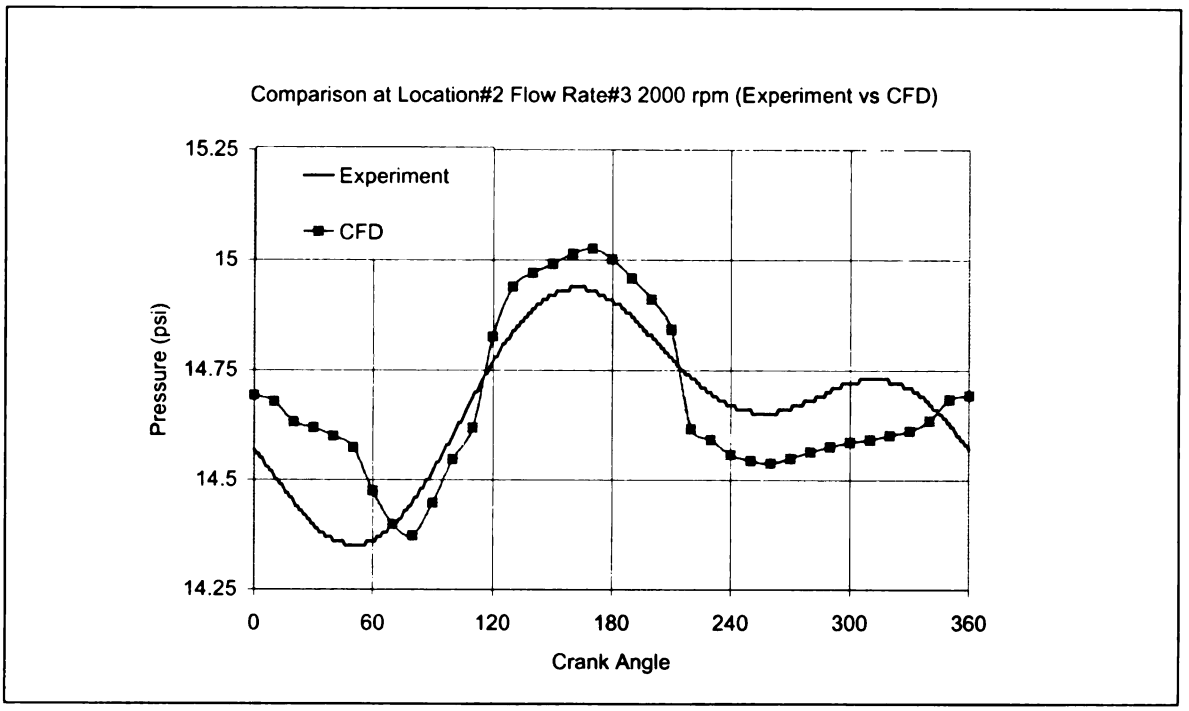

Figure 84: Pressure Data Comparison at 2000 rpm (Location 2, Flow Rate 3)

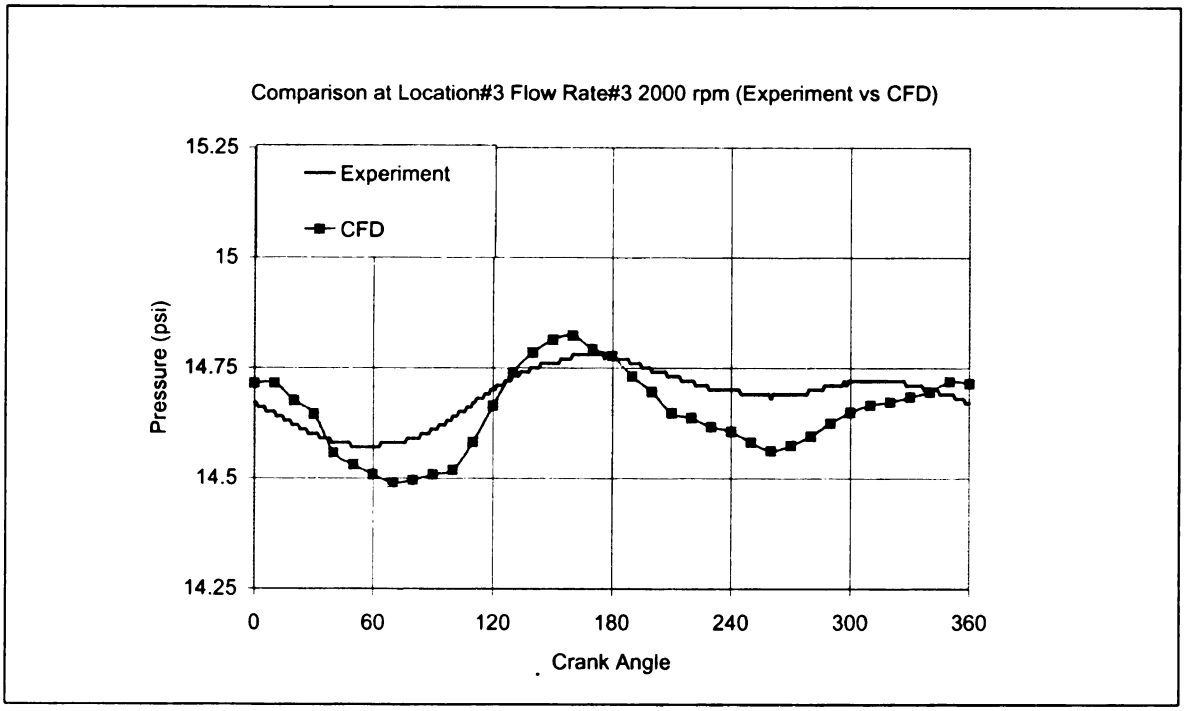

Figure 85: Pressure Data Comparison at 2000 rpm (Location 3, Flow Rate 3)

7.2.2 Comparison at 4000 rpm

The comparisons at 4000 rpm are shown from Figure 86 to Figure 94. The simulation results are compared with experimental data at every location and at each flow rate.

Both experimental and simulated results have the similar shape of a sine wave. The results for location 3 are better matched because it is near the inlet of the pipe, where the pressure always keeps at the atmosphere pressure.

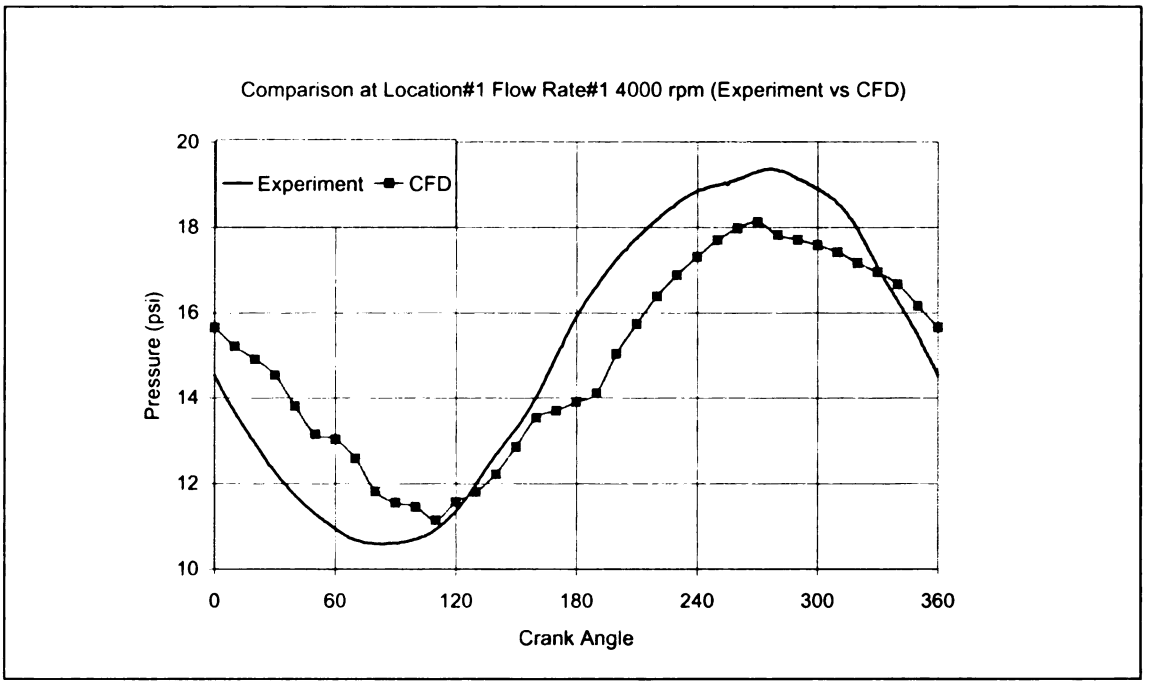

Figure 86: Pressure Data Comparison at 4000 rpm (Location 1, Flow Rate 1)

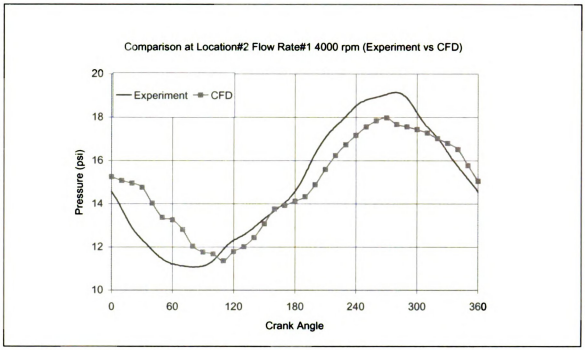

Figure 87: Pressure Data Comparison at 4000 rpm (Location 2, Flow Rate 1)

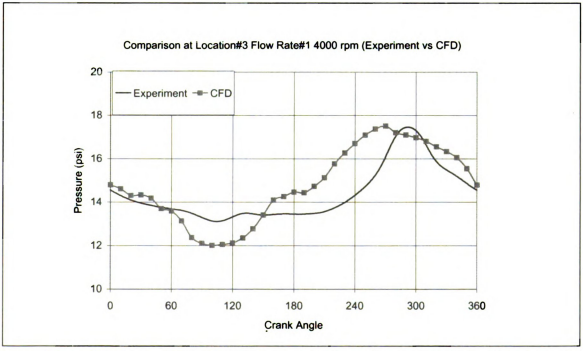

Figure 88: Pressure Data Comparison at 4000 rpm (Location 3, Flow Rate 1)

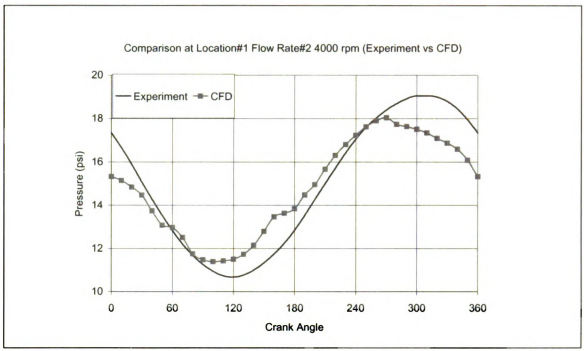

Figure 89: Pressure Data Comparison at 4000 rpm (Location 1, Flow Rate 2)

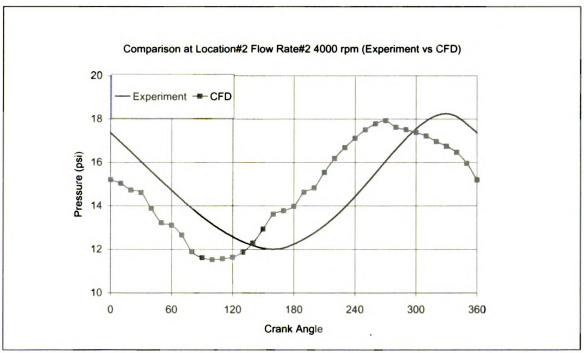

Figure 90: Pressure Data Comparison at 4000 rpm (Location 2, Flow Rate 2)

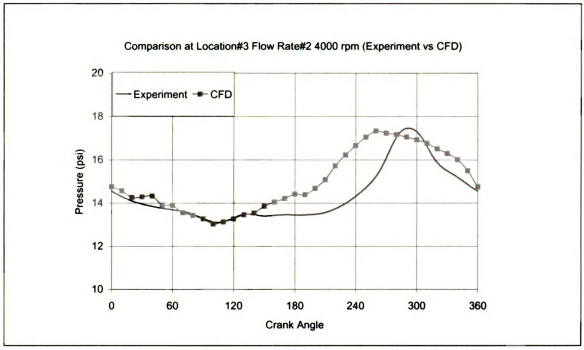

Figure 91: Pressure Data Comparison at 4000 rpm (Location 3, Flow Rate 2)

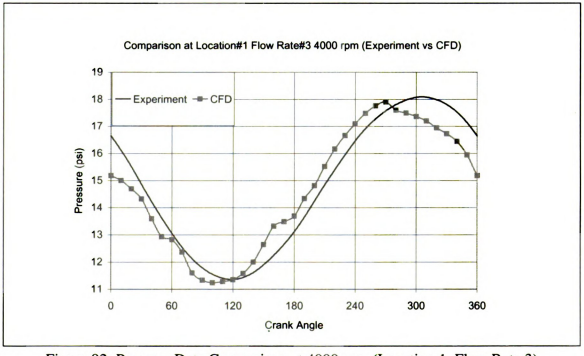

Figure 92: Pressure Data Comparison at 4000 rpm (Location 1, Flow Rate 3)

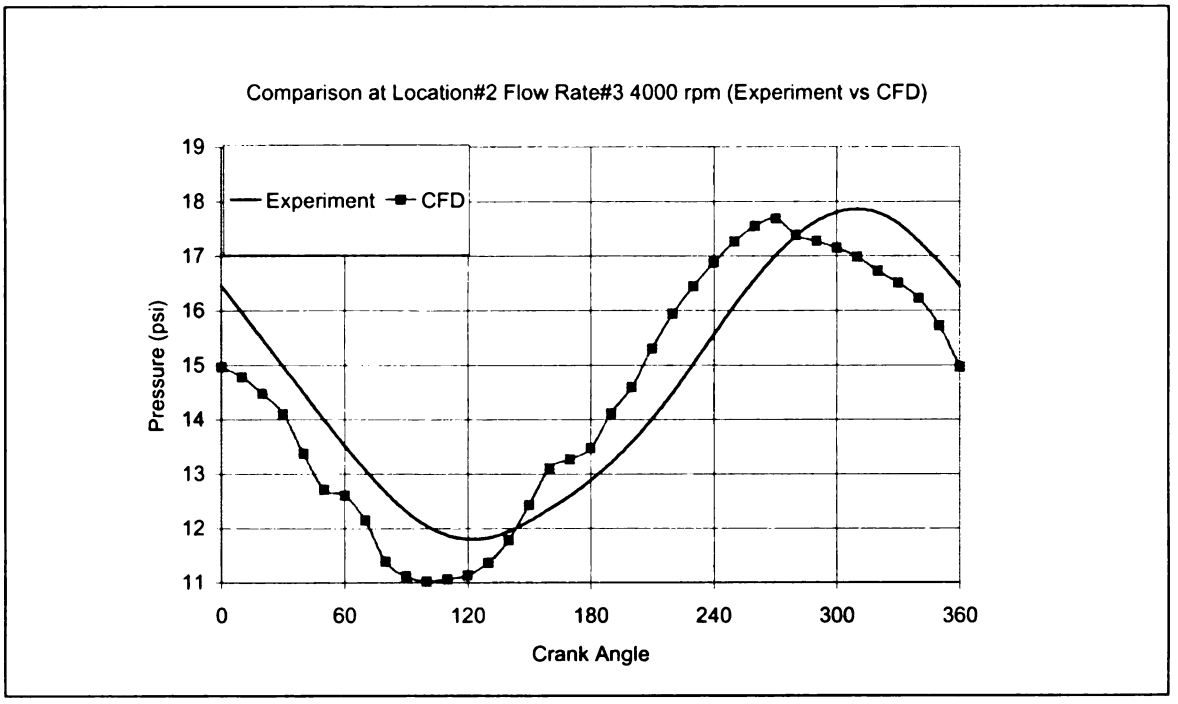

Figure 93: Pressure Data Comparison at 4000 rpm (Location 2, Flow Rate 3)

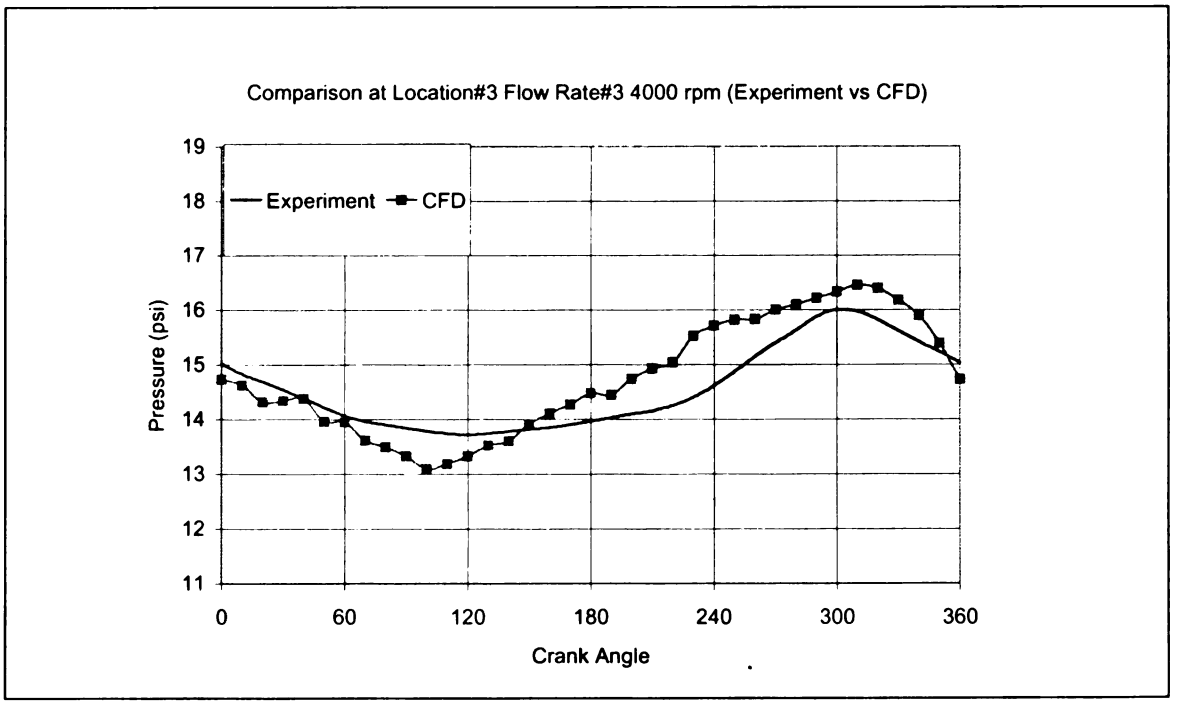

Figure 94: Pressure Data Comparison at 4000 rpm (Location 3, Flow Rate 3)

CHAPTER 8. SUMMARY AND CONCLUSIONS

The goal of this research was to develop a better understanding of the flow characteristics of the oscillating flow in the test region using both an experimental approach and a numerical simulation.

Laser Doppler Velocimetry (LDV) was used to measure the velocity profiles at three different locations and three flow rates. The test rig was operated at two engine speeds, 2000 rpm and 4000 rpm. The piezoresistive pressure sensor and amplifier were used to measure the pressure at three different locations under the same conditions.

Computations were performed to examine the velocity profiles and pressure in the oscillating flow system for different conditions. The simulation commences at BDC and continues for a time interval corresponding of 360 degree of crank revolution. Different engine speeds and different flow rates were investigated in the simulation.

The following conclusions can be drawn based on the results of this research.

1. The velocity profiles at the three different locations in the test region was measured at three different flow rates and two different engine speeds. The single component LDV system was proved to be a feasible method for measuring flow characteristics in an oscillating flow.
2. The pressure measurements were conducted at the three different locations in the test region at the same conditions as the test conducted for the LDV measurements. The results plotted as a function of crank angle show how the pressure wave moves in this test assembly.

3. The velocity profiles in the region of the orifice as a function of crank angle were investigated in the simulation. During the 2000 rpm runs, the vacuum pressure at the orifice made the flow all the way down from the top of the pipe without recirculation. As the engine speed increased to 4000 rpm, a recirculation region formed near the orifice.
4. Direct comparison of velocity and pressure results was analyzed under the same conditions. The 2000 rpm high flow rate data showed a 50% maximum difference from the theoretical velocity data and a 30% maximum difference from the theoretical pressure data.
5. The 4000 rpm high flow rate data showed a 60% maximum difference from the theoretical data and a 30% maximum difference from the theoretical pressure data.

LIST OF REFERENCES

[1] Peyret, R. and Taylor, T. D. [1983]. Computational Methods for Fluid Flow, Springer-Verlag, New York.

[2] Lee, K., Novak, M. and Schock, H., 3-D LDV Measurement of In-Cylinder Air Flow in a 3.5L Four-Valve SI Engine, SAE Paper No. 950648, 1995

[3] Hwang, K., Lee, K., Mueller, J., Stuecken, T. and Schock, H., Dynamic Flow Study in a Catalytic Converter Using Laser Doppler Velocimetry and High Speed Flow Visualization, SAE Paper No. 950786, 1995.

[4] Hascher, H., Kasser, J., Novak, M., Lee, K. and Schock, H., An Evaluation of Turbulent Kinetic Energy for the In-Cylinder Flow of a Four-Valve 3.5L SI Engine Using 3-D LDV Measurements, SAE Paper No. 970793, 1997.

[5] Kasser, J., Hascher, H., Novak, M., Lee, K. and Schock, H., Tumble and Swirl Quantification within a Motored Four-Valve SI Engine Cylinder Based on 3-D LDV Measurements, SAE Paper No. 970792, 1997.

[6] Watanabe, H., Kurahashi, T. and Kojima, M., Flow Visualization and Measurements of Torque Converter Stator Blades Using a Laser Sheet Lighting Method and a Laser Doppler Velocimetry, SAE Paper No. 970680, 1997.

[7] Hascher, H.G., SChock, H.,Avanessian, O., Novak, J., Comparison of Modeled and Measured 3-D In-Cylinder Charge Motion Throughout the Displacement of a Four-Valve SI Engine, SAE Paper No. 2000-01-0000, 2000.

[8] Stephens, M.A., Shih, T. I.-P., Flow and Heat Transfer in a Smooth U-Duct with and without Rotation, JOURNAL OF PROPULSION AND POWER, Vol. 15, No.2, March-April 1999.

[9] Heywood, J., Internal Combustion Engine Fundamentals, McGraw-Hill, 1988.

[10] Shapiro, A.H., The Dynamics and Thermodynamics of Compressible Fluid Flow, The Ronald Press Company, 1983.